MATHIEU INSTABILITY OF A SPAR PLATFORM WITH MOORING AND RISERS

B. J. Koo[a], M. H. Kim[a*], R. E. Randall[a]

[a]*Ocean Engineering Program, Civil Engineering Department, Texas A&M University,*

College Station, TX 77843-3136, USA

Abstract

Mathieu instability for a spar platform arises when there is a harmonic variation in the pitch restoring coefficients caused by large heave motion and the period of the heave motion is half of the pitch natural period. The pitch restoring coefficient can be represented by a function of the displaced volume and the metacentric height of spar hull. Due to heave motion, the displaced volume and the metacentric height of the spar platform change in time and this heave/pitch coupling can be represented by Mathieu's equation. The objective of this study is to evaluate damping effects and hull/mooring/riser coupled effects on the principle instability. In the simulation, the heave/pitch coupling of the spar platform is considered using the modified Mathieu equation. The wave elevation effect on Mathieu instability is also investigated. The Mathieu instability of a practical spar platform is carefully checked by a series of systematic simulations and comparisons of many different scenarios. When heave resonance occurs at the heave natural period equal to half of the pitch natural period, Mathieu instability, a kind of lock-in phenomenon, actually arises to increase the pitch motion significantly. The available damping is found to be important in suppressing the instability. The results also show that the additional pitch restoring force from buoyancy-cans plays an important role in the spar Mathieu instability.

Key words:

spar platform, Mathieu instability, heave-pitch coupling, time-varying pitch restoring coefficient, hull-mooring-riser coupling, damping and wave-elevation effect.

---

[*] Corresponding author. Tel.:979-847-8710; fax: 979-8162

E-mail address:m-kim3@neo.tamu.edu

Introduction

The classical spar production platform is a large circular cylinder with constant cross section and with a draft of approximately 200 m. The justification for the use of this enormous hull is that because of the large draft the heave and pitch responses of the platform are small enough to permit installation of rigid risers with dry trees. One of the advantages of the spar platform (classical and truss spar) is that its natural frequency is not near the peak frequency of the dominant wave energy. However, second - order wave effects and wind loads can excite large - amplitude slowly - varying resonant motions and the corresponding riser and mooring line loading. The contribution of the second - order wave loads to the motions and tensions plays an important role in the platform design. Thus, a dynamic analysis based on a reliable technique including those effects should be used for analyzing spar production platform. (e.g. Ran et al. (1995), Mekha et al. (1995), Cao and Zhang (1996), Kim et al. (1997), and Ran and Kim (1997)) In this paper, Mathieu's instability of a classical spar is investigated for a regular wave environment and the typical (i.e. West Africa and North Sea) swell conditions. Swell waves with a 25-second peak period have been reported offshore West Africa and North Sea. Generally, a spar platform has a 27~30-second heave natural period and a 45~60-second pitch natural period, respectively. Due to heave and pitch motion characteristics of the spar platform, the spar heave natural period is near the peak period of swell waves and the pitch natural period is twice the peak period of swell waves. In this situation, the ratio between wave frequency heave motion and pitch natural period motion is in the range of the principle unstable zone of the Mathieu instability. The Mathieu instability of a spar platform has been studied by Haslum and Faltinsen (1999), Rho et al. (2002 and 2003) and Zhang et al. (2002). Haslum and Faltinsen (1999) investigated the Mathieu instability in pitch motion combined with extreme amplitude heave resonance using a model test and simplified calculations. They showed a stability diagram for Mathieu's equation without considering pitch damping effects. Rho et al. (2002) also studied Mathieu's instability by model test and numerical calculation. They performed model tests for a spar platform with a moon-pool, helical strakes, and damping plates. Their studies show that the additional damping from heave plates and helical strake reduce the heave motion and experimentally confirmed the heave/pitch coupled non-linear motion for spar platforms. Zhang et

al. (2002) extended their studies to include pitch damping effects and developed a damped Mathieu's stability diagram from Mathieu's equation. However, Haslum and Faltinsen's (1999), Zhang et al.'s (2002) and Rho et al.'s (2002) studies did not consider the effects of time-varying displacement. In Haslum's and Rho's studies, the hull/mooring/riser coupling effects are not considered. In the present study, both are included. In Haslum's and Rho's experiment, the spar model has relatively smaller KB (i.e. distance between buoyancy center and keel) compare to the real spar platform. However, in this study, we employed a practical spar platform design (e.g. Prislin et al, 1999, Ma et al., 2000, and Tahar, Ran and Kim, 2002). Fig. 1 shows inside of the spar platform. The objective of this study is to evaluate damping effects and hull/mooring/riser coupled effects on the principle instability. The effects of time-varying displacement due to relative wave and heave motions are also investigated. The Mathieu type instability for the spar platform is investigated for a long period regular wave environment as well as the West Africa and North Sea swell condition. Five different spar platforms are simulated with five different wave environments to capture the damping effects and hull/mooring/riser coupled effects on the principle instability.

Formulation

Description of Existing Numerical Model

In a time-domain coupled dynamic analysis, the mooring and platform dynamics are solved simultaneously as an integrated system. The hydrodynamic forces on the platform are evaluated by diffraction theory. The first-order wave forces, added mass and radiation damping, and the second order mean and difference frequency forces on the platform are evaluated by WAMIT (Lee et al., 1999). Due to the motion characteristics of the spar, the sum-frequency parts are not important, and thus are not included in the subsequent motion analysis. The wave-force LTF (linear force transfer function) and QTFs (quadratic force transfer functions) are calculated in the frequency domain, and then these forces are converted to the time domain using the two-term Volterra series expansion (e.g. Ran and

Kim, 1997). The frequency-dependent radiation damping is included in the form of a convolution integral in the time domain simulation.

For the static/dynamic analysis of the mooring and riser system, an extension of the theory developed for the dynamics of slender rods by Garrett (1982) is used in WINPOST. A brief summary of the finite element formulation for a slender line follows. Assuming no torque the linear momentum conservation equation with respect to a position vector $\vec{r}(s,t)$ that is a function of arc length (s) and time (t) is expressed as:

$$-(B\vec{r}\,'')''+(\lambda\vec{r}\,')'+\vec{q}=m\ddot{\vec{r}} \tag{1}$$

$$\lambda = T - B\kappa^2 \tag{2}$$

$$T = T_0 + P_e A_e - P_i A_i \tag{3}$$

where prime and dot denote spatial derivative and time derivative respectively, B is bending stiffness, T the local effective tension, κ the local curvature, m the mass per unit length, $\vec{q}$ the distributed force on the rod per unit length, T_0 the local tension, P_e the external pressures, P_i the internal pressures, and A_e and A_i are external and internal cross sectional areas. The scalar variable λ can be regarded as a Lagrange multiplier. If the rod is assumed to be inextensible, the following condition must be satisfied;

$$\vec{r}\,'\times\vec{r}\,' - 1 = 0 \tag{4}$$

If the rod is extensible, the following relation is used

$$\frac{1}{2}(\vec{r}\,'\cdot\vec{r}\,'-1)=\frac{T}{A_t E}\approx\frac{\lambda}{A_t E} \tag{5}$$

$$A_t = A_e - A_i \tag{6}$$

For these equations, the geometric nonlinearity is fully considered and there is no special assumption made concerning the shape or orientation of the mooring line, as long as the rod remains elastic. The benefit of this equation is that (1) is directly defined in the global coordinate system and does not require any transformations to the local coordinate system, (Kim et al., 1999). The normal component of the distributed external force on the rod per unit length, q_n, is given by the generalized Morison equation, (e.g. Paulling and Webster, 1986).

$$q_n = C_I \rho A_e \dot{v}_n + \frac{1}{2} C_D \rho D \left| v_{nr} \right| v_{nr} + C_m \rho A_e \ddot{r}_n \tag{7}$$

where C_I ,C_D and C_m are inertia, drag and added mass coefficient, and $\dot{v}_n$, v_{nr} and $\ddot{r}_n$ are normal fluid acceleration, normal relative velocity, and normal structure acceleration, respectively. The symbols ρ and D are fluid density and local diameter. In addition, the effective weight, or net buoyancy, of the rod is included in q_n as a static load.

To develop the finite element formulation, consider a single element of length L and use the following expression;

$$\vec{r}(s,t) = \sum_i A_i(s) \vec{U}_i(t) \tag{8}$$

$$\lambda(s,t) = \sum_m P_m(s) \lambda_m(t) \tag{9}$$

where A_i and P_m are interpolation functions defined on the interval $0 \le s \le L$. Using equation (8) and (9), equation (1) can be reduced to the following equation (10) by the Galerkin method and integration by parts (Garrett, 1982):

$$\int_0^L \left[B\vec{r}'' A_i'' + \lambda \vec{r}' A_i' - \vec{q} A_i + m\ddot{\vec{r}} A_i \right] ds = B\vec{r}'' A_i' \Big|_0^L + \left\{ \lambda \vec{r}' - \left(B\vec{r}'' \right)' \right\} A_i \Big|_0^L \tag{10}$$

where it is assumed that the shape function A_i is continuous on the element. The first boundary term of the right-hand side is related to the moments on the ends, and the second term is the force on the ends, i.e. they are natural boundary conditions. If equation (4) is used, the result is:

$$\int_0^L P_m \left\{ \frac{1}{2} \left(\vec{r}' \cdot \vec{r}' - 1 \right) - \frac{\lambda}{A_i E} \right\} ds = 0 \tag{11}$$

The position vector, its tangent, and the Lagrange multiplier are selected to be continuous at a node between adjacent elements. The interpolation functions A_i and P_m are chosen to be Hermitian cubic and quadratic functions of s as follows;

$$A_1 = 1 - 3\xi^2 + 2\xi^3 \,,\; A_2 = \xi - 2\xi^2 + \xi^3 \,,\; A_3 = 3\xi^2 - 2\xi^3 \,,\; A_4 = -\xi^2 + \xi^3 \tag{12}$$

$$P_1 = 1 - 3\xi + 2\xi^2 \,,\; P_2 = 4\xi(1 - \xi) \,,\; P_2 = \xi(2\xi - 1) \tag{13}$$

where $\xi = s/L$. The parameters $\vec{U}$ and λ are thus:

$$\vec{U}_1 = \vec{r}(0,t),\ \vec{U}_2 = L\vec{r}'(0,t),\ \vec{U}_3 = \vec{r}(L,t),\ \vec{U}_4 = L\vec{r}'(L,t) \tag{14}$$

$$\lambda_1 = \lambda(0,t),\ \lambda_2 = \lambda(L/2,t),\ \lambda_3 = \lambda(L,t) \tag{15}$$

Elements are combined using the continuity of $\vec{r}$, $\vec{r}'$ and λ . The natural boundary conditions between two elements are canceled out, and leaving those conditions applicable at the ends of the rod. The upper ends of these tethers and mooring lines are connected to the hull through a generalized elastic spring that can also model both fixed and hinged conditions at its limit. The forces and moments proportional to the relative displacements are transmitted to the hull at the connection points. The transmitted forces from mooring lines to the platform are given by

$$\tilde{F}_P = \tilde{K}(\tilde{T}\tilde{u}_P - \tilde{u}_I) + \tilde{C}(\tilde{T}\dot{\tilde{u}}_P - \dot{\tilde{u}}_I) \tag{16}$$

where $\tilde{K}$ is the stiffness matrix, $\tilde{C}$ is the damping matrix, $\tilde{T}$ is the transformation matrix between the platform origin and connection point, and $\tilde{u}_P$ and $\tilde{u}_I$ are displacement vectors of the platform and connection point.

The buoyancy-can effect inside of the spar moon-pool developed by Koo (2003). Koo (2003) modeled the multiple-contact coupling between risers and riser guide frames using nonlinear gap spring model. The detailed derivation of the buoyancy-can effect inside of the spar moon-pool is available in Koo (2003). The additional restoring force from risers inside of the spar moon-pool using cubic spring model can be described by

$$\tilde{F}_R = \tilde{K}(\tilde{T}\tilde{u}_P - \tilde{u}_R)^3 \tag{17}$$

where $\tilde{u}_R$ is the displacement vectors of the contact point of the riser. The Coulomb damping between riser guide frames and risers inside of the spar platform modeled by

$$\tilde{F}_C = \mu\, sgn(\tilde{T}\tilde{u}_{P3} - \tilde{u}_{R3})\sqrt{\tilde{F}_{R1}^2 + \tilde{F}_{R2}^2} \tag{18}$$

where $\tilde{u}_{P3}$ and $\tilde{u}_{R3}$ are the vertical displacement vector of the contact point of the riser guide frame and riser, μ is the frictional coefficient between riser and riser guide frame and $\tilde{F}_{R1}$ and $\tilde{F}_{R2}$ are the horizontal contact force between riser and riser guide frame.

The hull response equation is combined into the mooring-line equation in the time domain as follows;

$$(\tilde{M}+\tilde{M}_a(\infty))\ddot{\tilde{u}}_P+\int_0^{\infty}\tilde{R}(t-\tau)\dot{\tilde{u}}_P d\tau+\tilde{K}_H\tilde{u}_P=\tilde{F}_D+\tilde{F}^{(1)}+\tilde{F}^{(2)}+\tilde{F}_P+\tilde{F}_R+\tilde{F}_C+\tilde{F}_{WD} \qquad (19)$$

where $\tilde{M}$ and $\tilde{M}_a$ are structure mass and added mass, $\tilde{R}$ is the retardation function (inverse cosine Fourier transform of radiation damping), $\tilde{K}_H$ is the hydrostatic restoring coefficients, $\tilde{F}_D$ is the drag force matrix on the hull, $\tilde{F}^{(1)}$ and $\tilde{F}^{(2)}$ are the first- and second-order wave load matrix on the hull, $\tilde{F}_P$ is the coupling force matrix between mooring lines and platform, $\tilde{F}_R$ is the contact force matrix between risers and riser guide frames, $\tilde{F}_C$ is the Coulomb damping force matrix between risers and riser guide frames and $\tilde{F}_{WD}$ is the wave drift damping force matrix. The added mass at infinite frequency is obtained from the Kramers-Kroing relation. For the time series of $\tilde{F}^{(1)}, \tilde{F}^{(2)}$ and $\tilde{F}_{WD}$, a two-term Volterra series is used. From the above time domain equation of motion, the hull/mooring line/riser coupled analysis can be achieved.

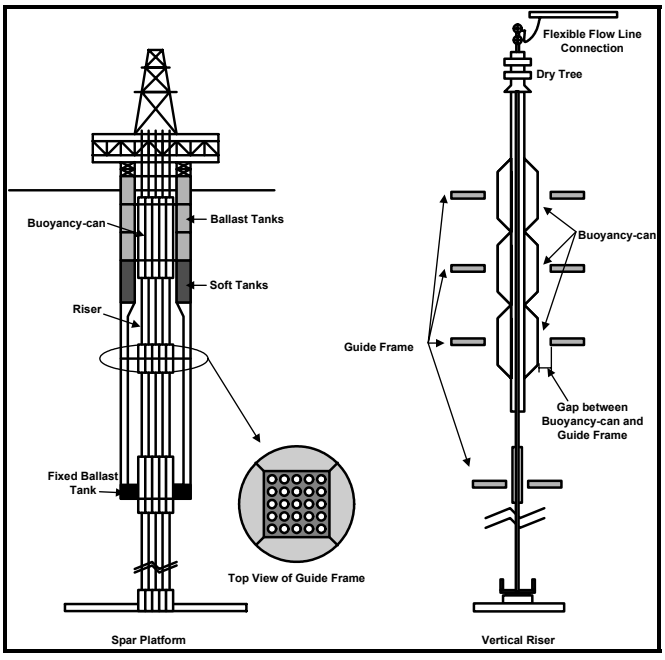

Fig. 1. Spar Hull, Buoyancy-can and Guide Frame.

Heave and Pitch Coupling of Spar Platform

For a spar, the pitch restoring stiffness K_{55} is a function of displaced volume and metacentric height $\overline{GM}$, represented by $\rho g \forall \overline{GM}$ in still water. When the spar has heave motion and the heave amplitude is ζ_3, then the metacentric height and displaced volume are changed with heave motion and wave elevation. The metacentric height and displaced volume can be obtained by:

$$\overline{GM}_{new} = \overline{GM} - \frac{1}{2}(\zeta_3(t) - \eta(x_c, y_c, t)) \tag{20}$$

$$\forall_{new} = \forall - A_w(\zeta_3(t) - \eta(x_c, y_c, t)) \tag{21}$$

where A_w is the spar water plane area, $\eta(x_c, y_c, t)$ is the wave elevation at center of flotation of the spar platform, x_c and y_c are the center of flotation. Based on a new metacentric height and displaced volume, the new pitch restoring stiffness, K_{55new}, can be calculated:

$$\begin{aligned} K_{55new} &= \rho g \forall_{new} \overline{GM}_{new} \\ &= K_{55} - \frac{1}{2}\rho g\left(\forall + 2A_w GM\right)\left(\zeta_3(t) - \eta(x_c, y_c, t)\right) + \frac{1}{2}\rho g A_w \left(\zeta_3(t) - \eta(x_c, y_c, t)\right)^2 \end{aligned} \tag{22}$$

Equation (22) clearly shows heave/pitch coupling and also shows time dependence of pitch stiffness. For simplicity, the heave motion is assumed to be a one-term harmonic and ignore the wave elevation effect, then heave motion can be expressed as $\zeta_3(t) = \zeta_3 \cos \omega t$, where ω is heave motion frequency. Thus, the pitch motion can be written as:

$$(I_{55} + A_{55})\ddot{\zeta}_5(t) + C_{55}\dot{\zeta}_5(t) + \rho g \forall (GM - \frac{1}{2}\zeta_3 \cos \omega t)\zeta_5(t) = 0 \tag{23}$$

where I_{55} and A_{55} are the pitch moment of inertia and the added pitch moment of inertia. ζ_5 and ζ_3 are pitch and heave motion respectively. Based on the new pitch equation (i.e. Mathieu's equation) of motion the parameter in the Mathieu's equation is defined as follows:

$$\alpha = \frac{\rho g \forall GM}{(I_{55} + A_{55})\omega^2} = \frac{\omega_5^2}{\omega^2} \tag{24}$$

$$\beta = \frac{0.5\rho g \forall \zeta_3}{(I_{55} + A_{55})\omega^2} \tag{25}$$

$$c = \frac{C_{55}}{(I_{55} + A_{55})\omega} \tag{26}$$

where, ω_5 is pitch natural frequency. Equation (23) through (26) are used for generate the damped Mathieu instability diagram. However, heave/pitch coupling of a spar platform cannot be simulated by the Mathieu equation due to wave elevation effects and submerged volume changes with time. Thus, in the time domain platform motion, equation (22) is used for K_{44new} and K_{55new} in Mathieu's instability investigation. The resultant formulation (i.e. modified Mathieu equation) for pitch equation of motion in the time domain simulation can be expressed as:

$$(I_{55} + A_{55})\ddot{\zeta}_5(t) + C_{55}\dot{\zeta}_5(t) + \rho g \forall_{new}(GM - \frac{1}{2}(\zeta_3(t) - \eta(x_c, y_c, t))\zeta_5(t) = 0 \tag{27}$$

Mathieu Stability Diagram

The Mathieu equation is a special case of Hill's equation that is a linear equation with a periodic coefficient. The standard form for Hill's equation is:

$$\ddot{x} + (\alpha + p(t))x = 0 \tag{28}$$

When p(t) is periodic, then it is known as Hill's equation. For the special case $p(t) = \beta \cos t$,

$$\ddot{x} + (\alpha + \beta \cos t)x = 0 \tag{29}$$

it is referred to as the undamped Mathieu's equation. A general damped Mathieu's equation is shown as follows:

$$\ddot{x} + c\dot{x} + (\alpha + \beta \cos t)x = 0 \tag{30}$$

This kind of nonlinear ordinary equation cannot be solved explicitly. However, by fixing the damping coefficient, zeros of infinite determinants can be found by specifying α (or β) and searching for the corresponding β (or α) that gives a set of results sufficiently close to zero. Two methods are available to find the parameter values for the parametric plane. The first is using the perturbation method and the second is using Hill's infinite determinants method. Using Hill's infinite determinants, the parametric curves can be obtained by the complex Fourier series. The first periodic solution of period 2π is as follow:

$$x(t) = \sum_{n=-\infty}^{\infty} s_n e^{int} \tag{31}$$

After substituting equation (31) into the damped Mathieu's equation, equation (30), the solution for all t is:

$$\sum_{n=-\infty}^{\infty} e^{int}\left\{\frac{1}{2}\beta s_{n+1}+(\alpha+inc-n^2)s_n+\frac{1}{2}\beta s_{n-1}\right\}=0 \tag{32}$$

This can be satisfied only if the coefficients are all zero:

$$\frac{1}{2}\beta s_{n+1}+(\alpha+inc-n^2)s_n+\frac{1}{2}\beta s_{n-1}=0\,, \quad n=0,\pm 1,\pm 2,.... \tag{33}$$

This infinite set of homogeneous equations for $\{s_n\}$ has non-zero solutions if the infinite determinant formed by the coefficients is zero, when $\alpha \neq n^2$ for any n. The infinite determinant is formed as:

$$\begin{vmatrix} . & . & . & . & . & . & . \\ . & \gamma_1 & 1 & \gamma_1 & 0 & 0 & . \\ . & 0 & \gamma_0 & 1 & \gamma_0 & 0 & . \\ . & 0 & 0 & \gamma_1 & 1 & \gamma_1 & . \\ . & . & . & . & . & . & . \end{vmatrix}=0 \tag{34}$$

where

$$\gamma_n=\beta/2(\alpha+inc-n^2),\quad n=0,1,2,.... \tag{35}$$

The second periodic solution of period 4π is determined by using

$$x(t)=\sum_{n=-\infty}^{\infty} s_n e^{\frac{1}{2}int} \tag{36}$$

After substituting equation (36) into damped Mathieu's equation, equation (30), the solution for all t is represented as:

$$\sum_{n=-\infty}^{\infty} e^{int}\left\{\frac{1}{2}\beta s_{n+2}+(\alpha+\frac{1}{2}inc-\frac{1}{4}n^2)s_n+\frac{1}{2}\beta s_{n-2}\right\}=0 \tag{37}$$

This can be satisfied only if the coefficients are all zero:

$$\frac{1}{2}\beta s_{n+2}+(\alpha+\frac{1}{2}inc-\frac{1}{4}n^2)s_n+\frac{1}{2}\beta s_{n-2}=0\,, \qquad n=0,\pm 1,\pm 2,.... \tag{38}$$

This infinite set of homogeneous equations for $\{s_n\}$ has non-zero solutions if the infinite determinant formed by the coefficients is zero; when $\alpha \neq n^2$ for any n. The infinite determinant is formed as:

$$\begin{vmatrix} . & . & . & . & . & . & . \\ . & \gamma_2 & 1 & \gamma_2 & 0 & 0 & 0 \\ . & 0 & \gamma_1 & 1 & \gamma_1 & 0 & 0 \\ . & 0 & 0 & \gamma_1 & 1 & \gamma_1 & 0 \\ . & 0 & 0 & 0 & \gamma_2 & 1 & \gamma_2 \\ . & . & . & . & . & . & . \end{vmatrix} = 0 \tag{39}$$

where

$$\gamma_{2n+1} = \beta / 2(\alpha + \frac{1}{2} i(2n+1)c - \frac{1}{4}(2n+1)^2), \quad n = 0,1,2,.... \tag{40}$$

The parametric plane generated by Hill's infinite determinant method is shown in Fig. 2 that shows that the second unstable region is more influenced by the damping effect than the principal unstable region. The damped Mathieu diagram also shows that when the damping is added to the system, the unstable regions separate from the α - axis. This means that the unstable region is reduced when damping is added to the system. However, when the principal unstable region is less influenced by damping, the principal unstable region should be examined carefully.

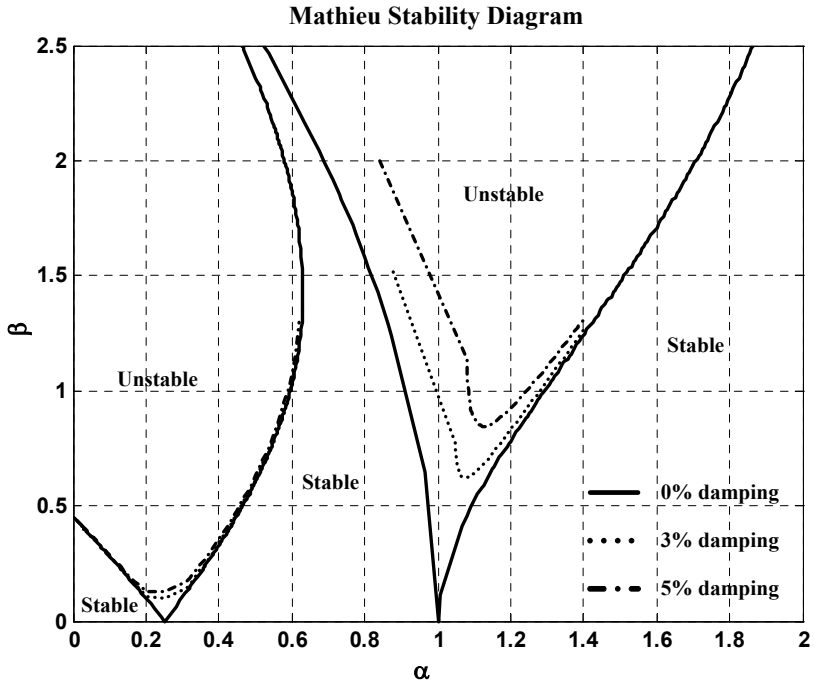

Fig. 2. Stability diagram for damped Mathieu's equation.

Description of Case Study

The specifications of the spar platform used in the present study are summarized in Table 1. The spar platform has 14 chain-wire-chain mooring lines and 23 steel vertical risers. The arrangement of mooring lines and risers are shown in Fig. 3. The mooring line characteristics are shown in

Table 2. The spar platform has 18 production risers, 1 drilling riser, 2 water injection risers, 1 oil export and 1 gas export riser, and the riser characteristics are tabulated in Table 3. In the regular wave simulation, four different spar hull drag coefficients (Table 4) are used to capture the pitch damping effects on the Mathieu instability.

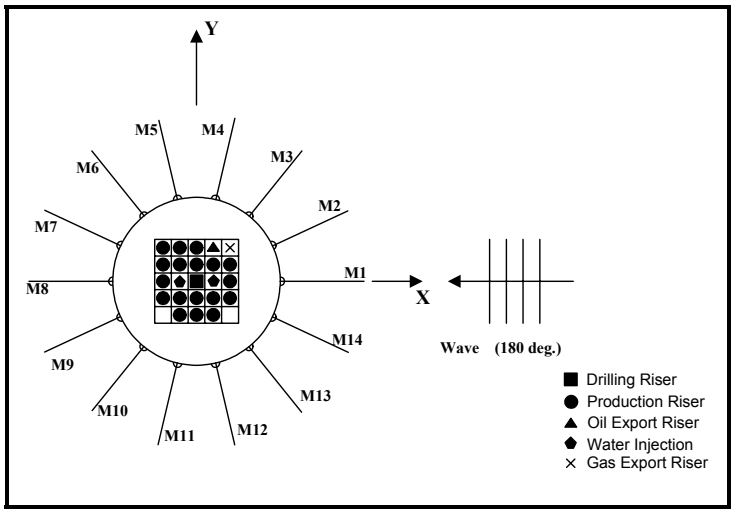

Fig. 3. Mooring lines/risers configuration and wave directions.

Table 1. Spar hull characteristics.

Classical Spar 914.4m (3000ft)	
Total Displacement (N)	2.163E9
Draft (m)	198.12
Hard Tank Depth (m)	67.06
Well Bay Dimension (m^2)	17.7 x 17.7
KB (m)	164.6
KG (based on Total Displacement) (m)	89.71
Radius of Gyration (based on Total Displacement) (m)	67.36(pitch), 8.69(yaw)
Drag Force Coefficient	1.0
Center of Pressure for Wind Area (m)	22
Design Depth (m)	914.4

Table 2. Spar mooring system characteristics.

Mooring Lines	Dry/Wet weight (N/m)	AE (KN)	Added mass (N/m)
133.4 mm K4 Studless Chain	3.71E+02 / 3.23E+02	1.33E+06	4.82E+01
136.5 mm Sheathed Wire	9.91E+01 / 1.98E+01	1.63E+06	1.98E+01

Table 3. Riser system characteristics.

Riser	No.	Top Tension (KN) At Keel/At Top of Spar	AE (KN)	Dry/Wet Weight (N/m)
Drilling	1	3.269E+03 / 4.167E+03	1.201E+07	5.95E+02 / 3.66E+02
Production	18	2.106E+03 / 2.344E+03	2.994E+06	3.01E+02 / 1.95E+02
Water Injection	2	1.362E+03 / 1.443E+03	1.837E+06	1.03E+02 / 6.46E+02
Oil Export	1	1.738E+03 / 1.872E+03	4.626E+06	2.96E+02 / 1.63E+02
Gas Export	1	8.870E+02 / 9.53E+02	4.626E+06	2.08E+02 / 7.54E+01

Table 4. Drag coefficient of the spar platform.

Designation	CASE	Quantities
Drag coefficient (without mooring lines and risers)	**CASE A**	0 (pitch damping 0.03%)
	CASE B	0.5 (pitch damping 1.0%)
	CASE C	2.5 (pitch damping 3.0%)
Drag coefficient (with mooring lines and risers)	**CASE D** **CASE E**	1.5

Description of Case Study and Environmental Conditions

The simulation is conducted for five different spar platforms with three regular wave environments and two swell wave environments. It is well known that pitch damping of a spar platform is around 1% ~ 4% of the pitch critical damping and depends on the pitch motion amplitude. Thus, simulations are conducted in 0.03% ~ 3.52% pitch damping ratio. Table 6 summarizes the period and wave amplitude used in the regular wave simulation. In the regular wave simulation, the comparison can be divided into three categories. The first category is a comparison study for pitch damping effects on Mathieu instability. The second category is the comparison between no hull/mooring/riser coupling effects versus hull/mooring/riser effects on Mathieu instability. Because the mooring lines and risers are completely removed from Case A, Case B and Case C, the spar platform pitch damping ratios are artificially changed by using different drag coefficients for each spar platform. A zero drag coefficient is used in

Case A, 0.5 drag coefficient is used in Case B, and 2.5 drag coefficient is used in Case C. Thus, Case A only considers radiation damping in the pitch direction. All the spar platforms use a heave plate with 1.5 drag coefficient to simplify the comparison study. All mooring lines and risers are considered in Case D and Case E, and these cases use 1.5 drag coefficient for the hull. The difference between the Case D and Case E is the riser modeling. The Case D spar uses a truncated riser at the keel and Case E uses fully modeled riser inducing the portion inside the moon-pool. Thus, the buoyancy-can effect and Coulomb damping effects are considered in Case E. In the simulation, Case A, B and C are considered as freely floating structures. Systematic comparisons between the five different spar platforms are used to show the damping effects and hull/mooring/riser coupled effects on Mathieu instability. The last category is the comparison study for including wave elevation effects. The submerged volume and the metacentric height of the spar platform are also changed by wave elevation. If the incident wave elevation is large and the spar heave motion has a phase difference with the wave elevation then the wave elevation effect cannot be ignored. Thus, in the time domain simulation, the relative heave motion is calculated and compared to the heave motion without wave elevation effect. The swell wave conditions are summarized in Table 7. To generate the swell wave time series, a JONSWAP spectrum is used in the simulation with a value of 6.0 used for the over shooting parameter. CASE E is used in the swell environment conditions and the Mathieu instability is checked based on regular wave simulation results.

Table 5. Summary of the spar platforms used in case study.

	Damping Ratio (%) Pitch/heave	**Mooring**	**Riser**	**Coulomb Damping**
CASE A	0.03 / 0.7	w/o	w/o	w/o
CASE B	1.0 / 0.7	w/o	w/o	w/o
CASE C	3.0 / 0.7	w/o	w/o	w/o
CASE D	3.3 / 2.72	w	w/t	w/o
CASE E	3.3 / 3.44	w	w/f	w
Notes: w/o = without consideration; w = with consideration w/t = consider riser as truncated model, w/f = consider riser as fully modeled				

Table 6. Regular wave condition.

	T (sec)	Wave amplitude (m)
RW-A	26.0	6.00 ~7.00
RW-B	27.8	1.50 ~ 7.00
RW-C	22.7	7.00
Notes:RW = regular wave		

Table 7. Swell environment condition.

	Hs (m)	Tp (sec)	γ
Swell-A	2.5	23	6.0
Swell-B	1.7	25	6.0

Numerical Results and Discussion

Free Decay Simulation

To evaluate the heave and pitch damping ratio and natural period of the spar platform, free decay simulations are conducted. Fig. 4 shows the pitch free decay simulation results. To capture the different damping ratio, different drag coefficients are given for each spar hull. In Case A, the spar hull drag coefficient is 0.0 thus, only radiation damping is considered in this case. Case B and C use 0.5 and 2.5 drag coefficient so that the spar damping ratio is 1.0% and 3.0% respectively. As mentioned before, Case D and E use the same drag coefficient but different riser modeling. The fully modeled riser (Case E) has a small pitch natural period and slightly larger damping ratio compared with truncated riser model (see Table 8) because of the effects of riser-gap contact. Fig. 5 shows the heave free decay results for all cases. In the Case E simulation, the spar platform initially tilted in pitch and roll directions, and it has additional damping from Coulomb friction. The results (see Table 9) show that most of the heave damping in a classical spar platform comes from the mooring lines. From free decay simulation results, it is interesting to notice that the heave damping from the mooring lines is important for the classical spar platform. The heave damping from coulomb friction is relatively small but not negligible. The results shows that, heave natural period of

the spar platform is half of the pitch natural period except for Case E, thus strong Mathieu instability is expected in the heave resonance zone.

Based on this free decay test, pitch and heave damping effects on the principle unstable zone in the Mathieu instability are investigated in the following regular wave simulation.

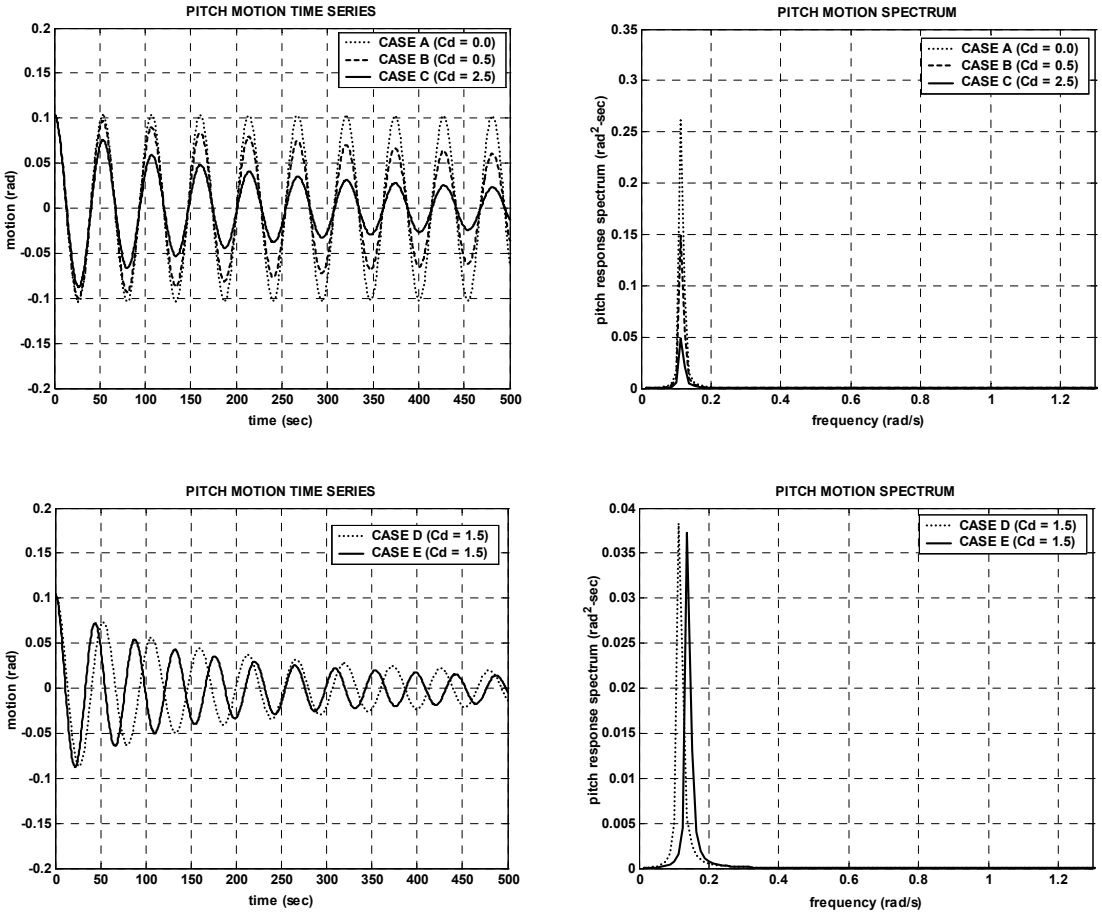

Fig. 4. Pitch free decay simulation results.

Table 8. Pitch motion natural periods and damping ratios.

	CASE A	CASE B	CASE C	CASE D	CASE E
T_N (sec)	57.6	57.6	57.6	57.6	45.5
ς (%)	0.03	1.01	2.99	3.28	3.52

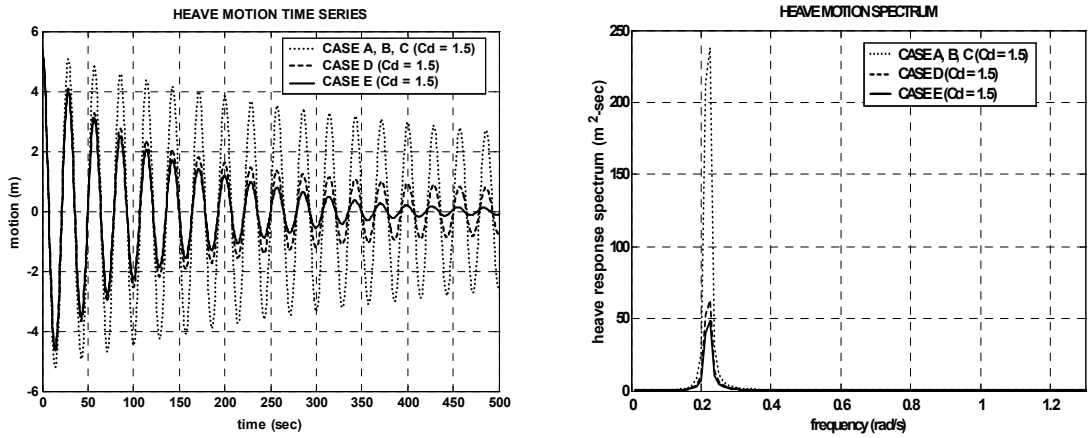

Fig. 5. Heave free decay results.

Table 9. Heave motion natural periods and damping ratio.

	CASE A	CASE B	CASE C	CASE D	CASE E
T_N (sec)	27.8	27.8	27.8	27.8	27.8
ς (%)	0.77	0.77	0.77	2.72	3.44

Mathieu's Instability in Regular Waves

Slightly Off Resonance –Slightly Off Instability Condition

The results of regular wave simulation A (RW-A) are shown in Table 10, Table 11, Fig. 6 and through Fig. 12. To capture the Mathieu instability, simulations are conducted with varying wave amplitudes. In 6.0-meter regular wave amplitude simulation, the Mathieu instability is triggered in Case A and B. Fig. 6 shows the result from the Case A spar platform. Fig. 6 clearly shows that pitch motion is drastically increased after 2000 seconds. The pitch response spectrum, Fig. 6, shows the largest peak exists in the pitch natural period zone even in the 26.0 seconds long period wave environment. It is interesting to notice that heave motion is also disturbed after the large pitch motion is started. This clearly shows that the wave energy transfers to heave and pitch motion turn by turn (see Fig. 7). Table 10 summarizes the statistical results from the simulation. The comparison between Case A and Case B statistical results,

in Table 10, show that the 1% pitch damping ratio is not enough to suppress the Mathieu instability. Thus, when the heave motion is larger than 8.0-meter the Mathieu instability is triggered in Case A and B. However, 8.0-meter heave motion is not enough to trigger the Mathieu instability in Case C mainly because of large pitch damping. On the other hand, Fig. 8 shows spar heave and pitch motion without time varying pitch hydrostatic coefficient (i.e. constant pitch hydrostatic restoring coefficient), and this result shows that constant pitch hydrostatic restoring coefficient can not generate the Mathieu instability and significantly underestimates the pitch motion of the spar platform. To clarify Mathieu instability, the detailed time series are shown in Fig. 7. The pitch motion time series shows that the pitch motion is stable up to 1000 sec. The pitch time series in Fig. 7 shows that the pitch motion has the same period as the regular wave period (i.e. 26 sec) in first 1000 sec, but after 1000 sec the pitch motion is disturbed. The reason is that the large heave motion changes the pitch restoring moment. Fig. 7 shows that the pitch motion gradually increases by the superposition of two adjacent motion peaks and, it doubles the amplitude of pitch motion as well as period. After two pitch motion peaks are superposed, the pitch motion drastically increased because motion becomes the pitch natural period motion. Fig. 7 clearly shows that the Mathieu instability resemble the lock-in phenomena. When pitch motion is increased by Mathieu instability, the large pitch motion also disturbs the heave motion. Fig. 7 shows the disturbed heave motion for Case A, and Fig. 9 shows the pitch response time series for Case B Spar platform. It is interesting to notice that the Case B spar has Mathieu instability in pitch motion, but the tendency of pitch motions are different from Case A. This is caused by the damping effect on pitch motion. As mentioned before, the Case B and Case C spar platform have 1% and 3% damping ratio in pitch motion respectively. When Mathieu instability occurs in Case B, a 1% pitch damping maintains the pitch motion as stable rather than unstable. This tendency is also shown in experiment by Rho (2003). The results for Case D and Case E are shown in Fig. 11 and Fig. 12 and summarized in Table 11. Because Case D and Case E include the mooring lines and risers, a larger wave amplitude (= 7.0m) is used in the simulation. Fig. 11 shows that the damping from mooring lines and risers, and the result from Case D spar has the same tendency as Case C simulation. The Case C and D spar have a small disturbance in pitch motion (i.e. 3000 sec – 6000 sec), but the pitch motion of the Case E spar does not

show any disturbance in pitch motion. It is because the Case D spar uses the truncated riser model, consequently, does not change the pitch natural periods. However, Case E Spar considers buoyancy-can effect, and it can shift the pitch natural period. The buoyancy-can effects on the Mathieu instability are more clearly shown in the following RW-B simulation in which wave period in which wave period is even closer to the half of the pitch natural period with smaller incident wave heights.

Table 10. Comparison of the statistics (Regular wave simulation A).

RW A: T = 26 sec amp. = 6.0 m						
	CASEA		CASE B		CASE C	
	HEAVE	PITCH	HEAVE	PITCH	HEAVE	PITCH
UNIT	m	deg.	m	deg.	m	deg.
MEAN	7.03E-02	-5.94E-02	7.65E-02	-6.08E-02	7.92E-02	-6.55E-02
STD	5.05E+00	5.63E+00	5.49E+00	5.39E+00	5.61E+00	1.20E+00
EXE	8.23E+00	1.80E+01	8.23E+00	1.18E+01	8.23E+00	1.85E+00
Notes: STD = standard deviation; EXE = extreme						

Table 11. Comparison of the statistics (Regular wave simulation A).

RW A: T = 26 sec, amp. = 7.0 m				
	CASE D		CASE E	
	HEAVE	PITCH	HEAVE	PITCH
UNIT	m	deg.	m	deg.
MEAN	4.31E-02	-1.68E-01	-2.55E-02	-1.80E-01
STD	5.68E+00	1.43E+00	5.58E+00	1.65E+00
EXE	8.06E+00	-2.21E+00	7.94E+00	-2.51E+00
Notes: STD = standard deviation; EXE = extreme				

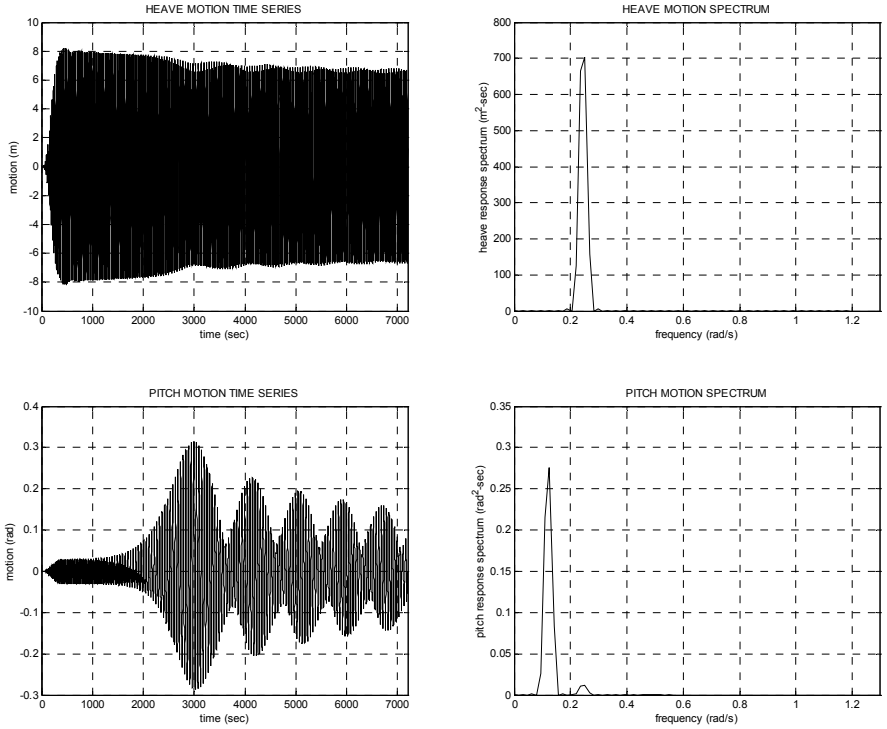

Fig. 6. Heave/Pitch motions (CASE A: T_p = 26 sec, amp. = 6.0 m).

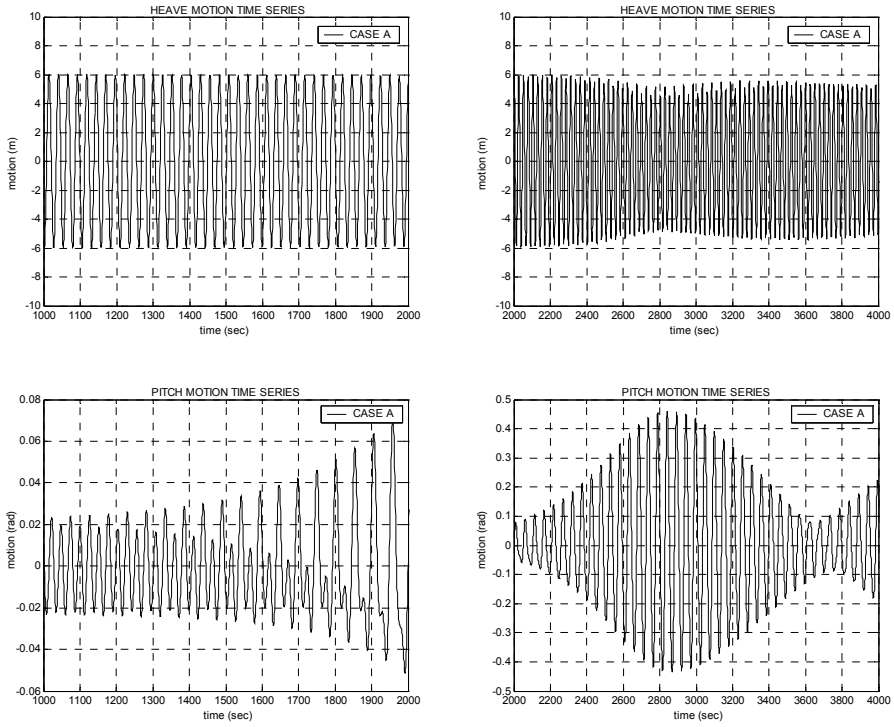

Fig. 7. Heave/Pitch response time series (1000 sec – 4000 sec).

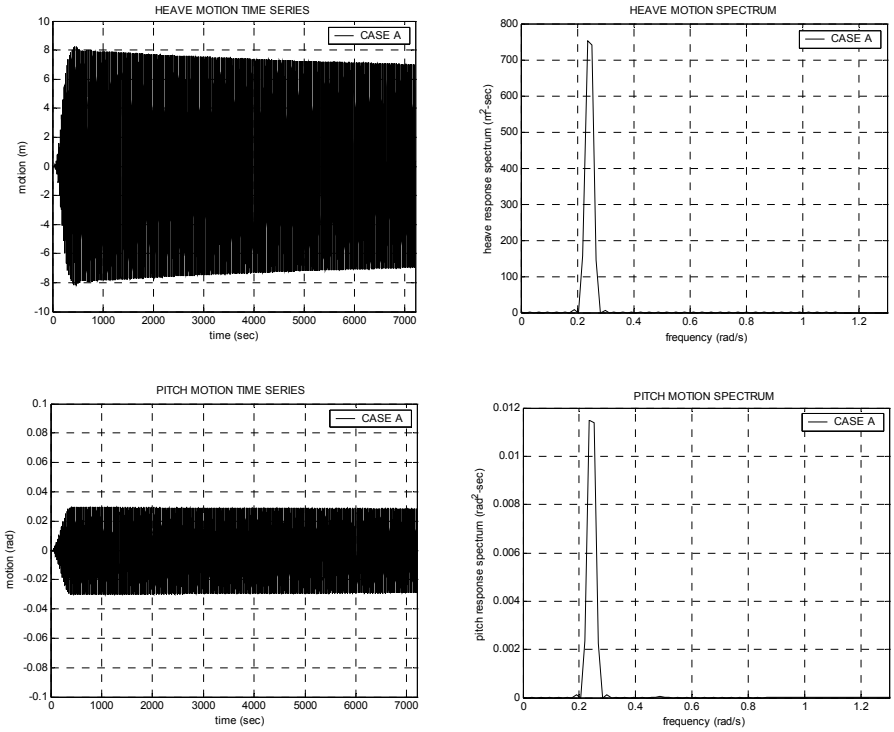

Fig. 8. Heave/Pitch motions without time varying restoring coefficient (CASE A: T_p = 26 sec, amp. = 6.0 m).

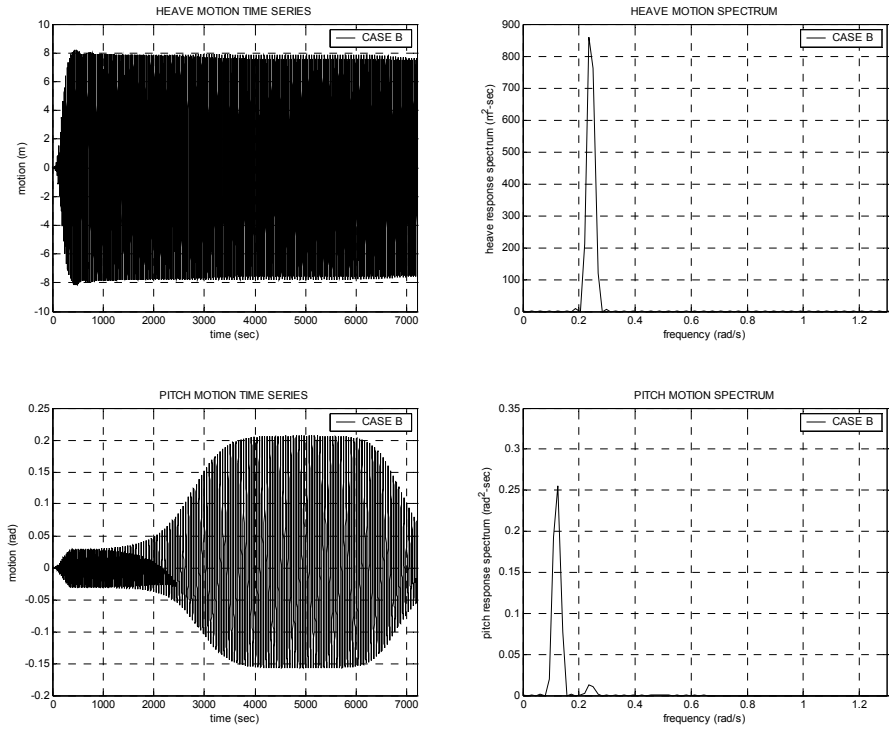

Fig. 9. Spar heave and pitch motions (CASE B: T_p = 26 sec, amp. = 6.0 m).

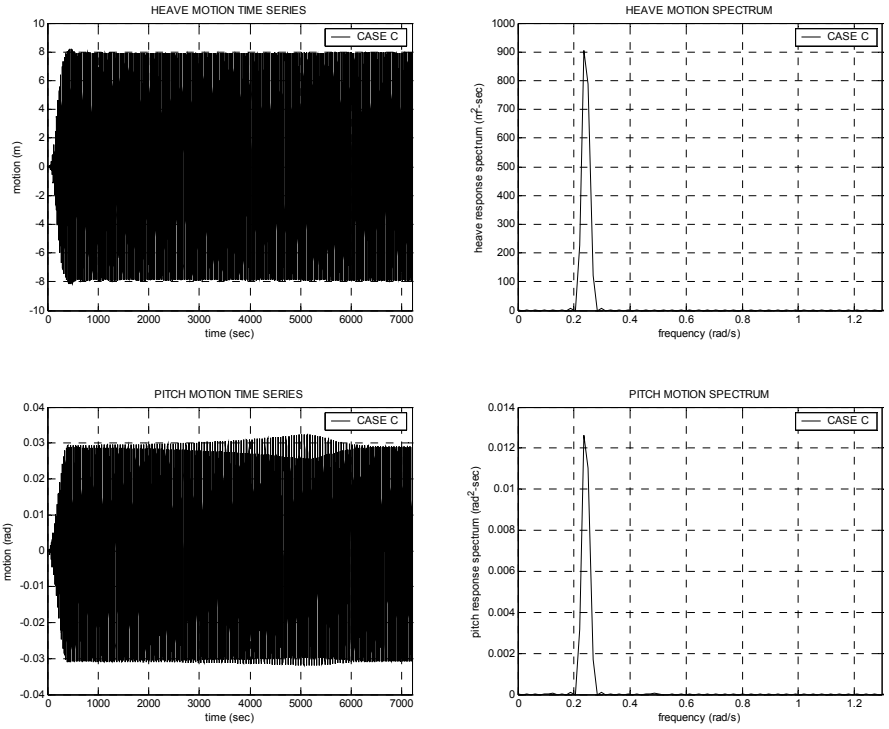

Fig. 10. Spar heave and pitch motions (CASE C: T_p = 26 sec, amp. = 6.0 m).

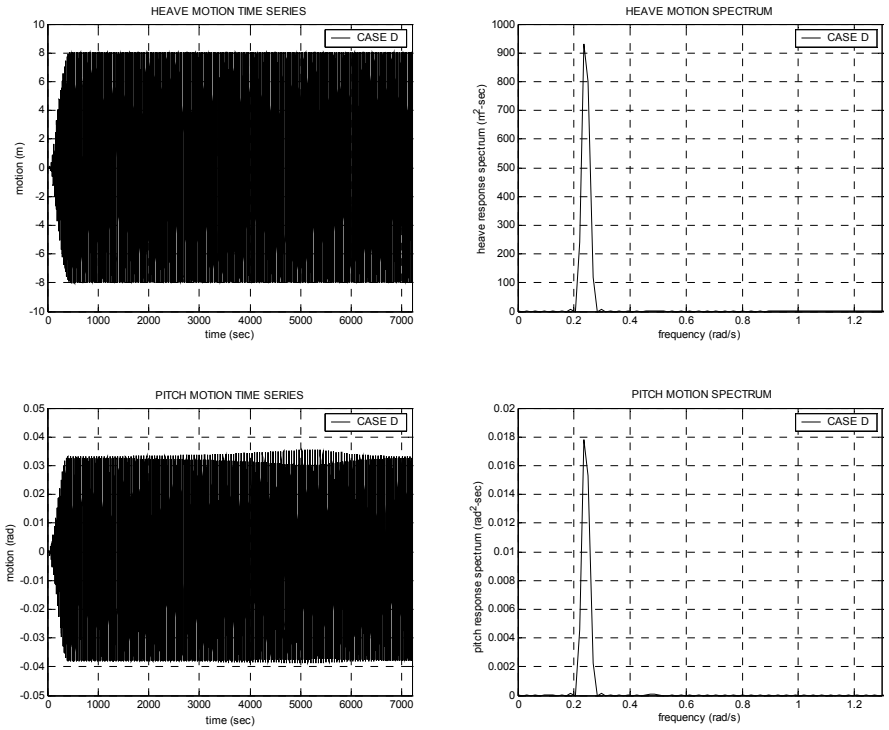

Fig. 11. Spar heave and pitch motions (CASE D: T_p = 26 sec, amp. = 7.0 m).

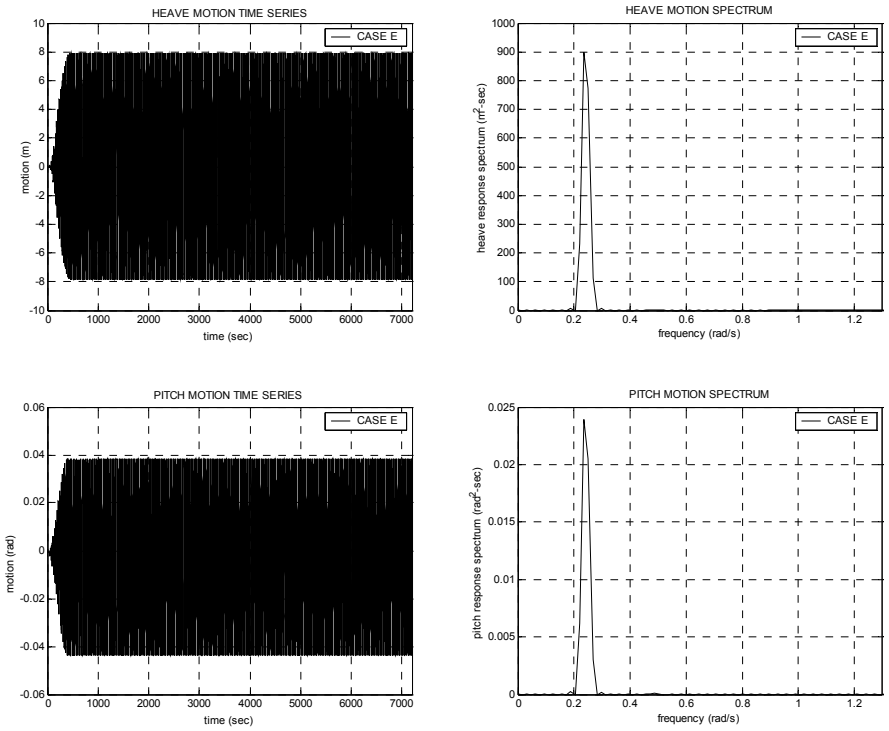

Fig. 12. Spar heave and pitch motions (CASE E: T_p = 26 sec, amp. = 7.0 m).

Heave Resonance Condition and T_{Pitch}/T_{Heave} very close to 1/2

To confirm the spar platform stability, the heave resonance zone is investigated in the RW-B simulation. As mentioned before, RW-B uses a 27.8 sec wave period and this wave period is exactly the same as the heave natural period and closer to half of the pitch natural period. The simulation results are shown in Fig. 13 through Fig. 18 and summarized in Table 12 and Table 13. In the simulation, the result from Case A spar platform is not available due to the absence of damping, thus unrealistically modeled. The Case B simulation results in Fig. 13 show that small amplitude waves generate heave motion larger than 8.0 m causing the Mathieu instability. This means that 1% pitch damping ratio is not enough to suppress the Mathieu instability. The CASE C spar simulation results in Fig. 14 show that the Case C spar also has Mathieu instability when heave motion is larger than 8.0 m. It is interesting to notice that, in RW-A case, the Case C spar does not exhibit Mathieu instability with 3% damping, but, in RW-B case, the Case C Spar has Mathieu instability. The reason is that, in RW-B case, the α factor is 0.25 where the most severe

Mathieu instability occurs. The Case C Spar in the 2.0 m wave amplitudes is shown in Fig. 15. The results show similar trend but the instability is triggered earlier. This means that 3% pitch damping ratio can keep the pitch resonance motion stable after the Mathieu instability is occurs.

The simulation results for the Case D and E spar platforms with larger wave amplitude (= 7m) are shown in Fig. 16 through Fig. 19. The Case D spar results show Mathieu instability due to large heave motion and 0.25 alpha factors. However, the detailed time series for pitch motion shows that Mathieu instability occurs after 2000 sec, but, due to pitch damping effect (3.3%), the superposition of two adjacent peaks cannot be fully developed as the resonant motion. It clearly shows that the pitch damping dampened the pitch resonance from Mathieu instability. The Mathieu instability is not triggered in the Case E spar even with a 11.3 m heave motion because the condition of Mathieu instability is not met that is the additional restoring moment from buoyancy-can effect changes the pitch natural period of motion and it avoids the critical α factor (i.e. 0.25). Fig. 18 clearly shows that the pitch motion of the Case E spar platform only has wave frequency motion. This result clearly shows the buoyancy-can pitch natural period shifting effects on Mathieu instability. It shows that in the same heave motion Case D has Mathieu instability but Case E does not have Mathieu instability. To ensure stability of Case E spar, a 22.7 second regular wave simulation is conducted. In the 22.7 sec wave period, Case E spar has 0.25 α factor. However, the results show that heave motion of the Case E Spar is not large even when a 7-meter wave amplitude is used. It can be attributed to the Coulomb damping from the contact of risers and riser guides. The RW-A and RW-B simulation results show that buoyancy-can effects play a very important role in Mathieu instability analysis for the spar platform. Thus, without proper modeling of risers and mooring lines in the simulation and experiment may lead to incorrect results under certain conditions. The wave amplitudes and periods used in the simulation are not practical unless long-period swells are involved but can be demonstrated in the laboratory (Rho et al. (2002)). Based on the regular wave simulation results, in the following section, Mathieu instability in a spar platform is checked for a swell environment.

Table 12. Comparison of statistics (Regular wave simulation B).

	RW B: T = 27.8 sec, amp. = 1.5				amp. = 2.0	
	CASE B		CASEC		CASE C	
	HEAVE	PITCH	HEAVE	PITCH	HEAVE	PITCH
UNIT	m	deg.	m	deg.	m	deg.
MEAN	7.40E-03	-2.11E-02	6.84E-03	-2.14E-02	1.24E-03	-2.65E-02
STD	4.82E+00	3.02E+00	4.82E+00	5.37E-01	6.11E+00	1.93E+00
EXE	-8.07E+00	-7.17E+00	-8.07E+00	-1.58E+00	9.83E+00	3.47E+00
Notes:STD = standard deviation; EXE = extreme						

Table 13. Comparison of statistics (Regular wave simulation B and C).

RW B: T = 27.8 sec, amp. = 7.0					T = 22.7	
	CASE D		CASE E		CASE E	
	HEAVE	PITCH	HEAVE	PITCH	HEAVE	PITCH
UNIT	m	deg.	m	deg.	m	deg.
MEAN	-2.55E-02	-3.20E-01	-1.52E-02	-3.28E-01	1.05E-01	-7.83E-02
STD	8.12E+00	2.87E+00	7.96E+00	2.01E+00	1.59E+00	1.58E+00
EXE	1.15E+01	-6.36E+00	1.13E+01	-3.15E+00	2.38E+00	-2.31E+00
Notes:STD = standard deviation; EXE = extreme						

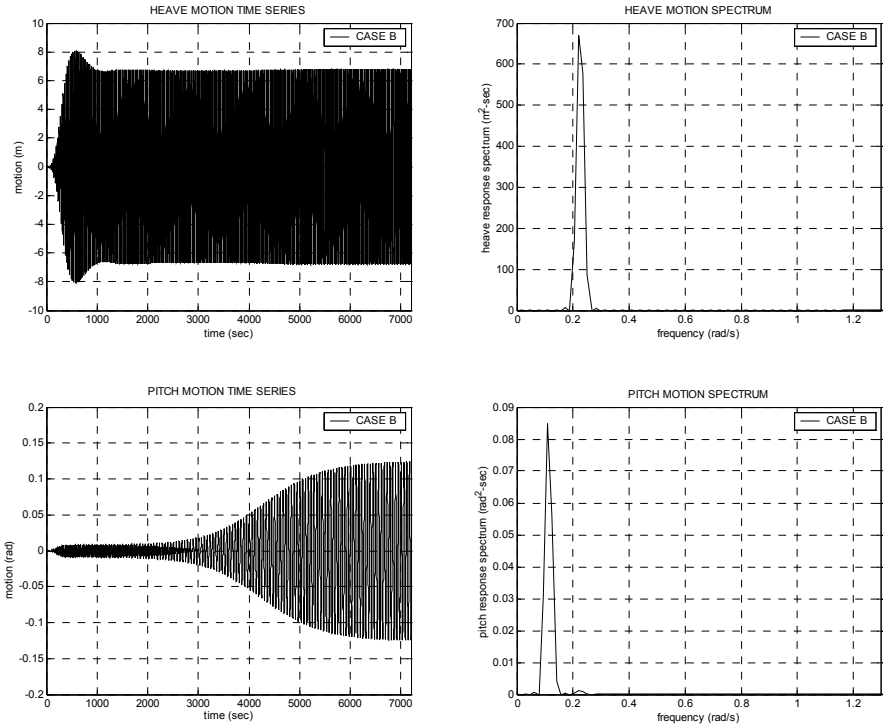

Fig. 13. Spar heave and pitch motions (CASE B: T_p = 27.8 sec, amp. = 1.5 m).

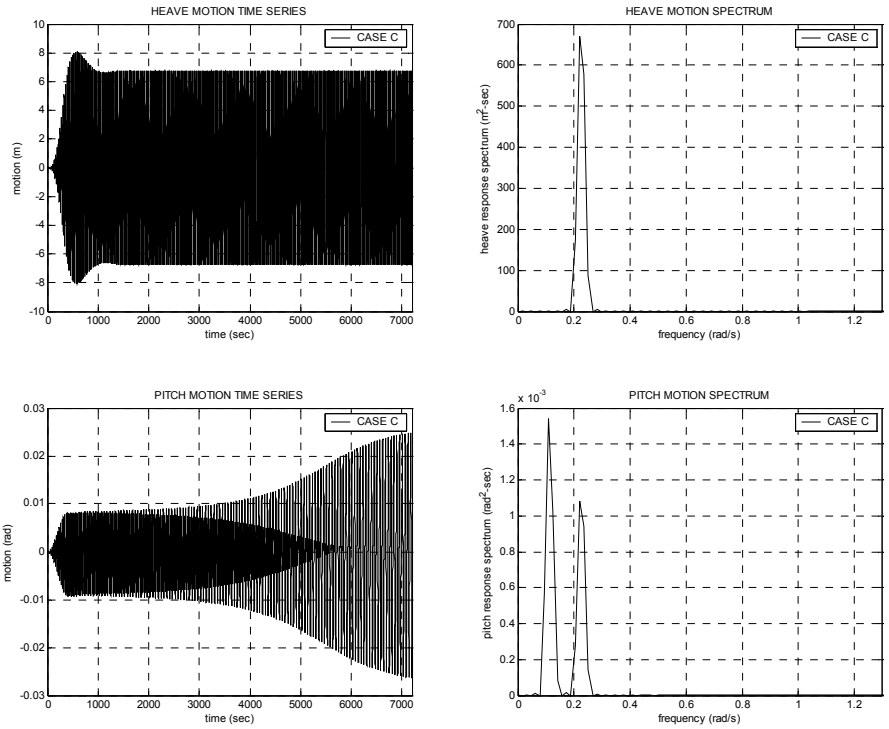

Fig. 14. Spar heave and pitch motions (CASE C: T_p = 27.8 sec, amp. = 1.5 m).

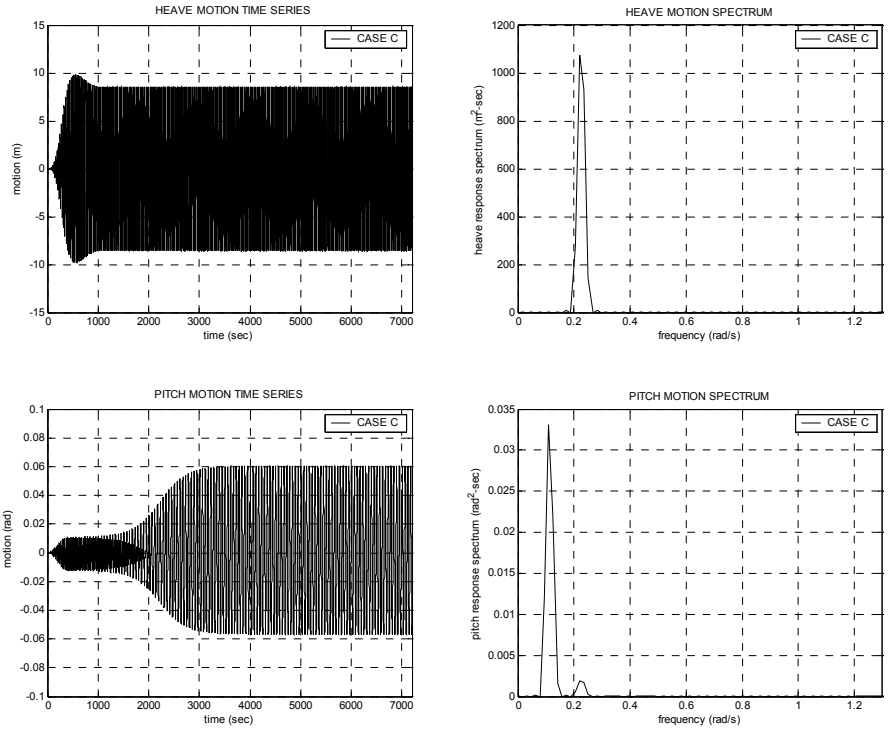

Fig. 15. Spar heave and pitch motions (CASE C: T_p = 27.8 sec, amp. = 2.0 m).

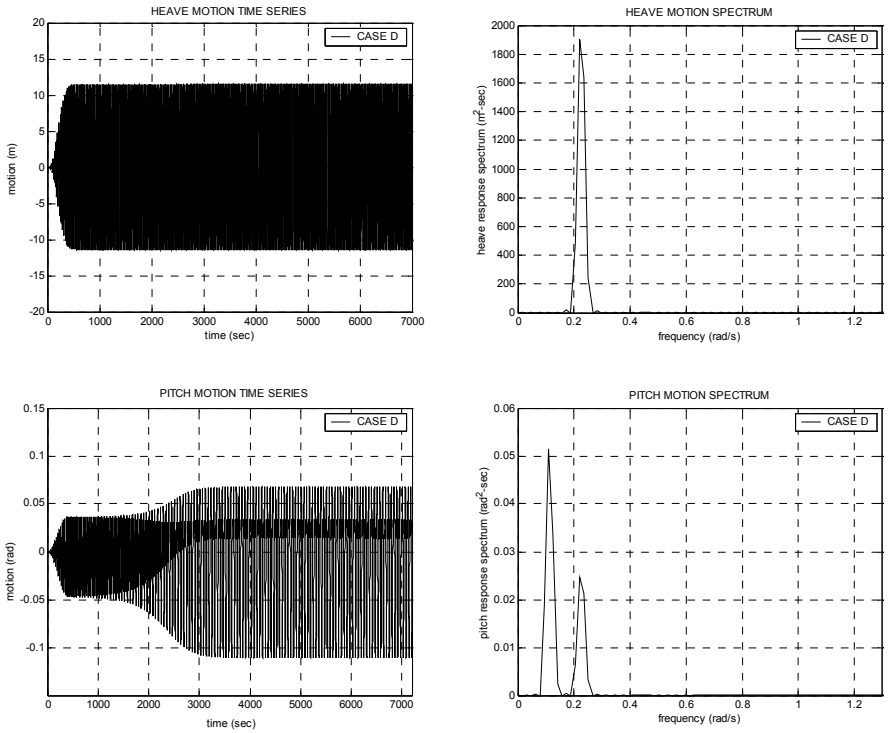

Fig. 16. Spar heave and pitch motions (CASE D: T_p = 27.8 sec, amp. = 7.0 m).

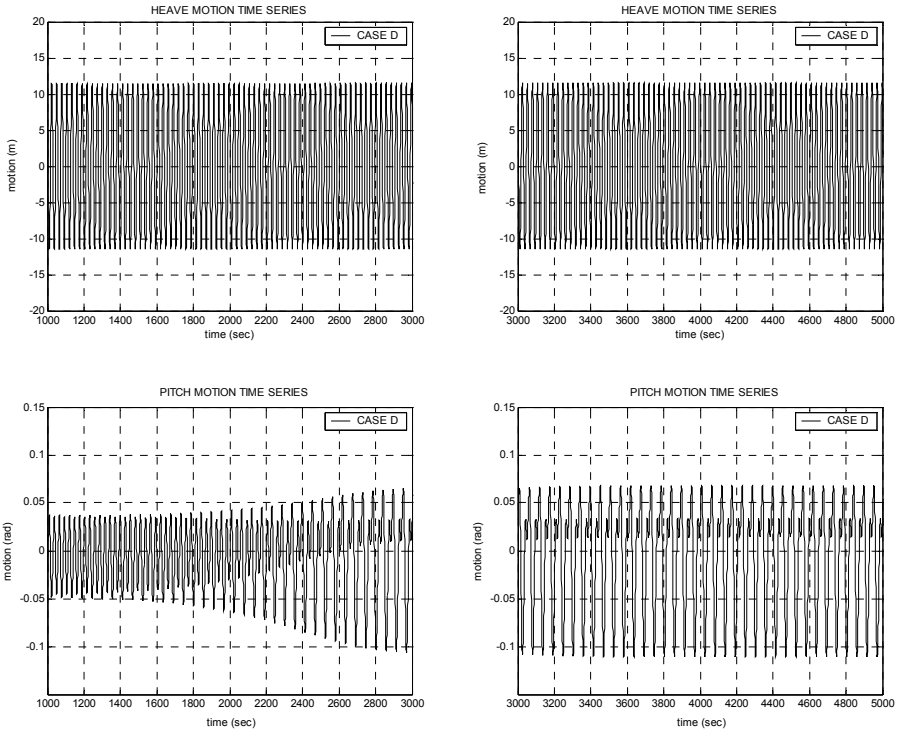

Fig. 17. Heave/Pitch response time series (1000 sec – 5000 sec).

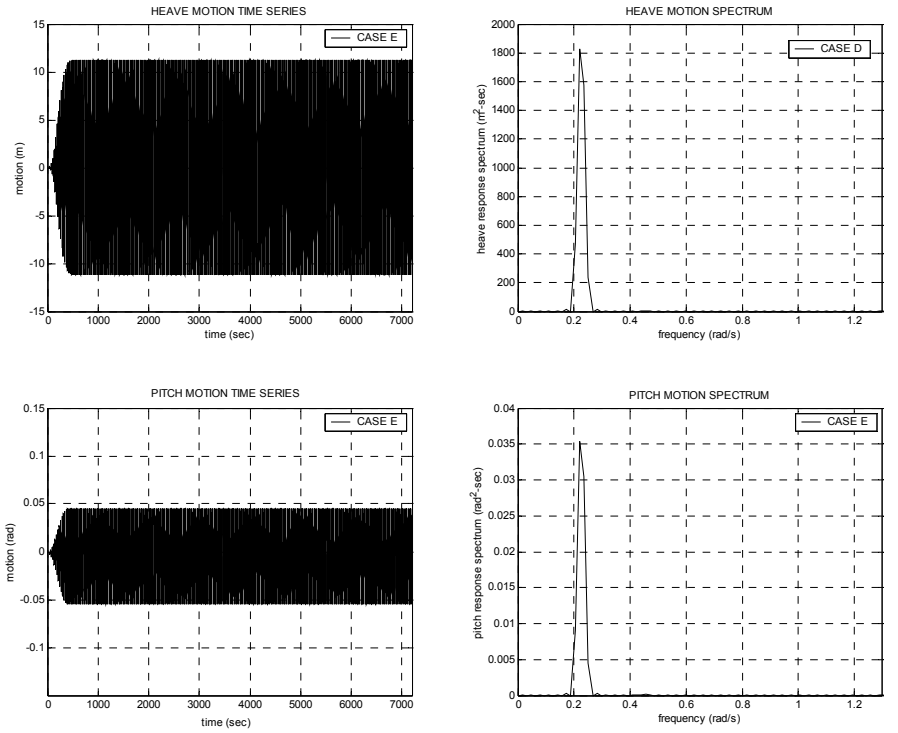

Fig. 18. Spar heave and pitch motions (CASE E: T_p = 27.8 sec, amp. = 7.0 m).

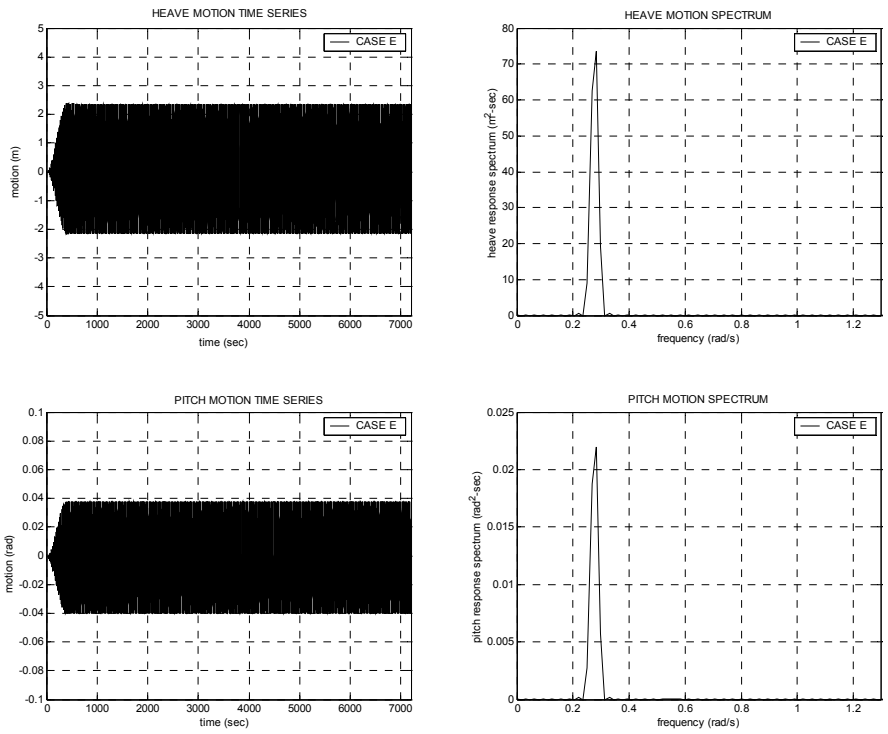

Fig. 19. Spar heave and pitch motions (CASE E: T_p = 22.7 sec, amp. = 7.0 m).

Wave Elevation Effect on Mathieu Instability

The results from RW-A and RW-B clearly show the pitch damping effects and hull/mooring/riser coupling effects on the Mathieu instability of the spar platform. The result of Case C spar platform in the RW-A simulation, the spar is very stable which means that 3% of pitch damping is large enough to suppress the Mathieu instability. However, the regular wave simulations (RW-A and RW-B) do not consider the wave elevation effect. If the wave elevation is not large then the wave elevation effect is not important, but if the wave elevation is large and the spar platform heave motion has phase difference with wave elevation then the submerged volume and metacentric height of the spar platform are significantly affected by wave elevation. To capture the wave elevation effects on the Mathieu instability, simulations are conducted for Case C spar in RW-A wave and Case E spar in 22.7 sec regular wave. The results are shown in Fig. 20 and Fig. 21. Fig. 20 shows that the wave elevation and heave motion have almost a 180 degree phase difference. Due to the phase difference, heave motion with respect to wave elevation is almost 14 m.

Thus, the results show that Mathieu instability is triggered in pitch motion. This result clearly shows the wave elevation effect on the Mathieu instability. Thus, in this situation (i.e. large wave amplitude and large phase difference), wave elevation effect has to be considered in the Mathieu instability analysis. However, Fig. 21 shows that Case E spar does not experience Mathieu instability. The reason is that the relative heave motion (= 9.0 m) is not large enough to trigger the Mathieu instability. It has been already shown in previous simulation (i.e. RW-B, Case E).

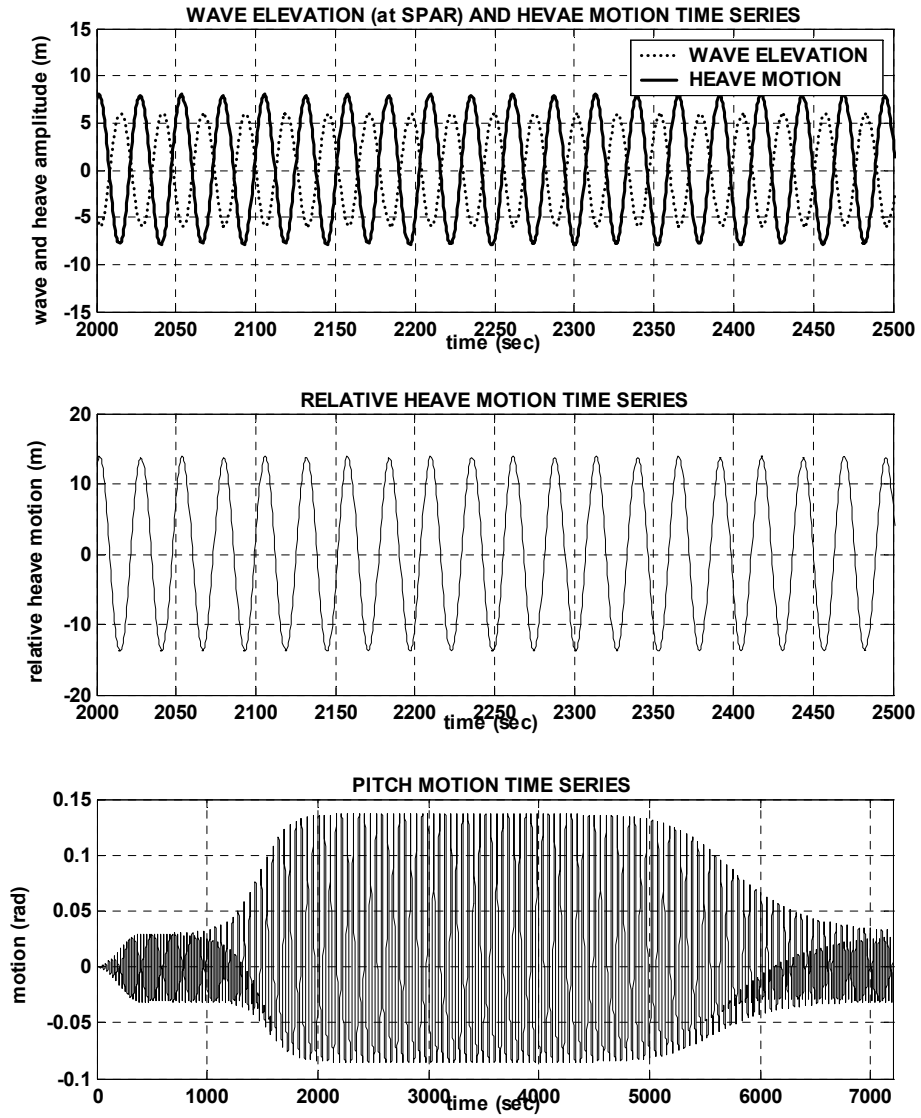

Fig. 20. Regular wave simulation results include wave elevation effect (CASE C: T_p = 26.0 sec, amp. = 6.0 m).

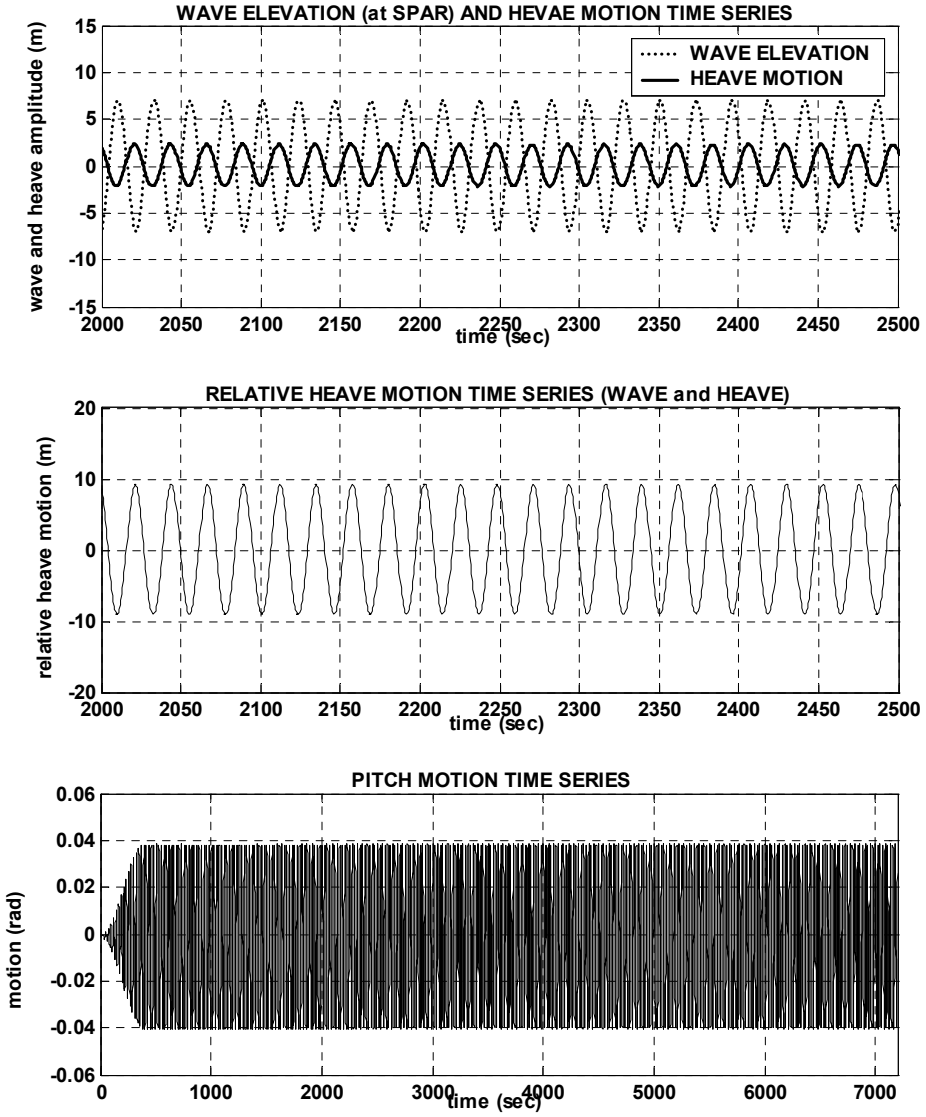

Fig. 21. Regular wave simulation results including wave elevation effect (CASE E: T_p = 22.7 sec, amp. = 7.0 m).

Mathieu Instability in Swell Condition

Fig. 22 and Fig. 23 show the swell wave spectrum and time series which are used in the simulation. The Swell-A and Swell- B (typical of West Africa and North Sea) simulation results are shown in Fig. 24 through Fig. 29 and summarized in Table 14 and Table 15. The wave elevation effect is considered in the swell wave simulation (Swell-

A and Swell-B). However, the wave elevations are not large in the swell wave environment, thus the wave elevation effect is not large. The maximum wave elevation is 2.4 m in Swell-A and 1.6 m in Swell-B. Based on the regular wave simulation (RW-A and RW-B), Mathieu instability is not triggered in CASE E Spar even in large heave motion. The Swell-A and Swell-B simulation results show that the maximum heave motion is around 1.7 ~ 1.9 m and maximum pitch motion is around 0.6 ~ 0.7 degree. The ranges of heave and pitch motion in the regular wave simulation results show that the spar platform is very stable. It shows that the spar platform does not have Mathieu instability in the swell wave environment. However, the heave motion standard deviation in the swell condition is five times larger when compare to that in 100-year hurricane condition. (Koo (2003))

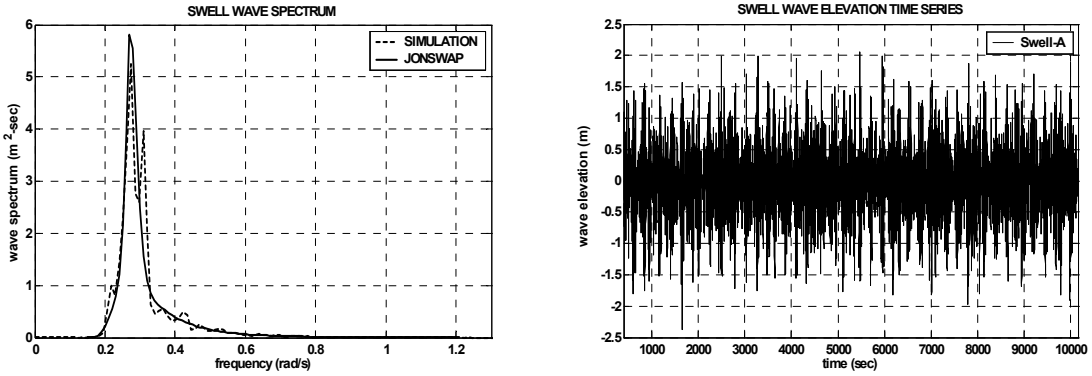

Fig. 22. Wave spectrum and time series for Swell – A.

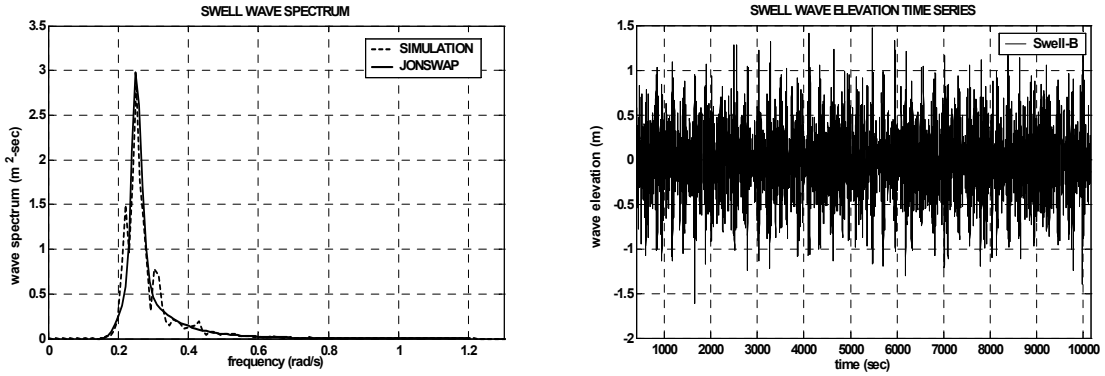

Fig. 23. Wave spectrum and time series for Swell – B.

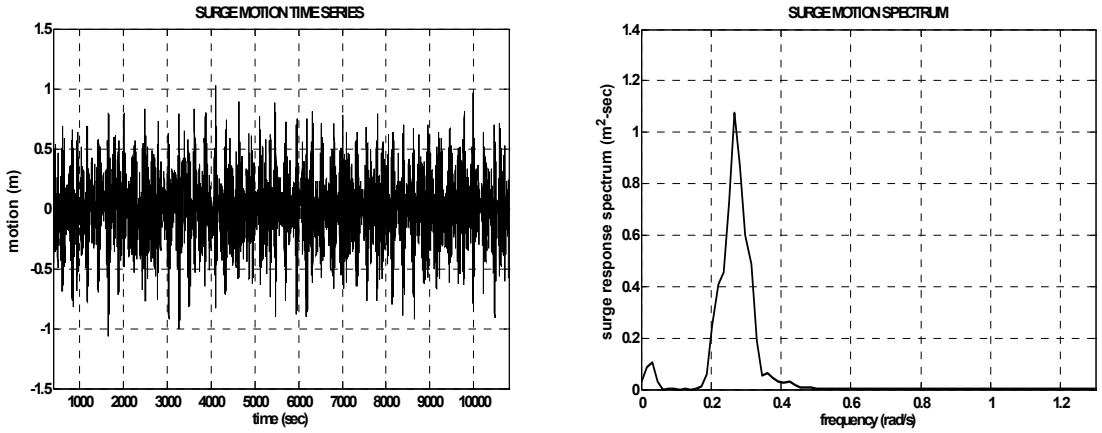

Fig. 24. Surge response time series and spectrum (Hs = 2.5 m, Tp =23 sec, γ =6.0).

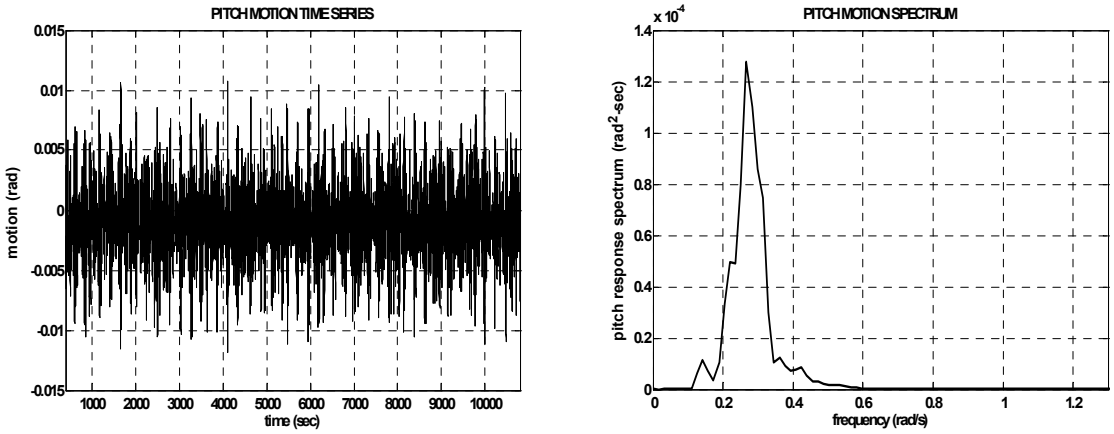

Fig. 25. Pitch response time series and spectrum (Hs = 2.5 m, Tp =23 sec, γ =6.0).

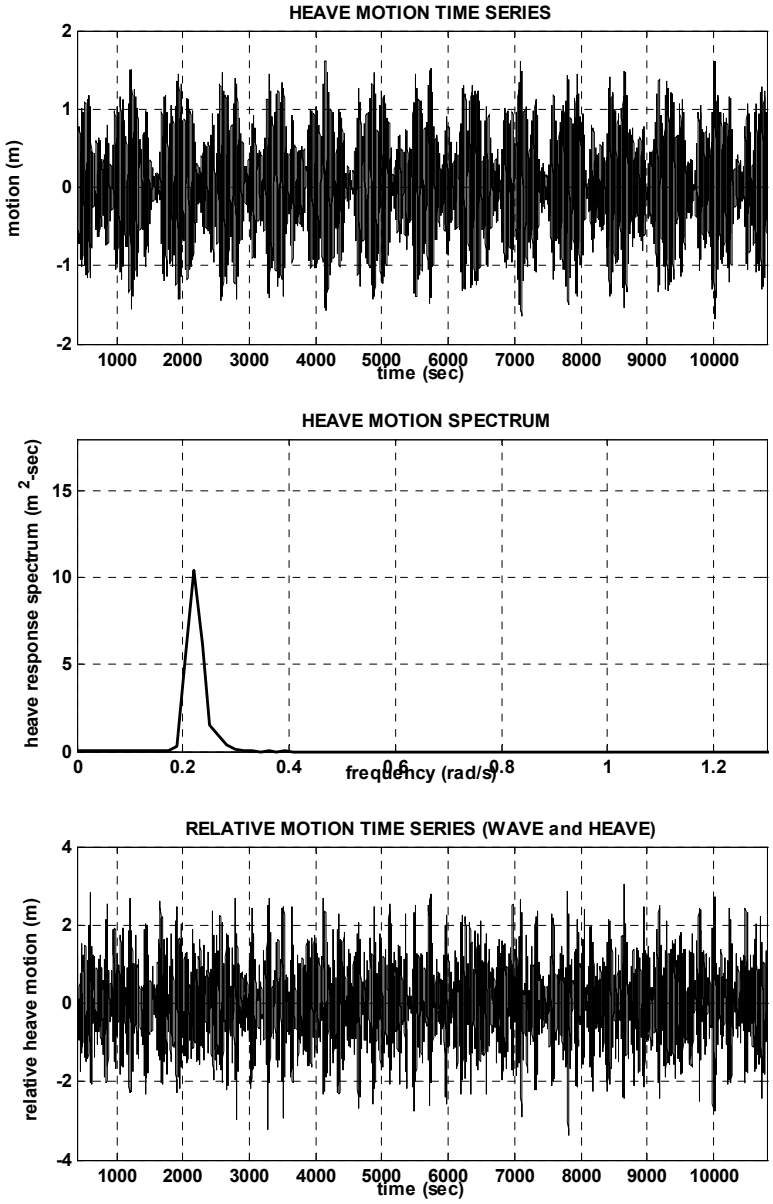

Fig. 26. Heave response time series and spectrum (Hs = 2.5 m, Tp =23 sec, γ =6.0).

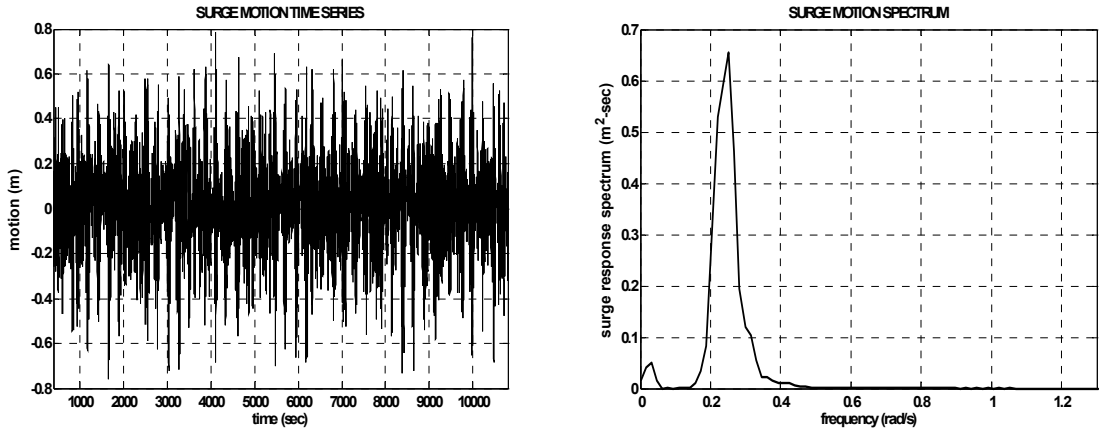

Fig. 27. Surge response time series and spectrum (Hs = 1.7 m, Tp =25 sec, γ =6.0).

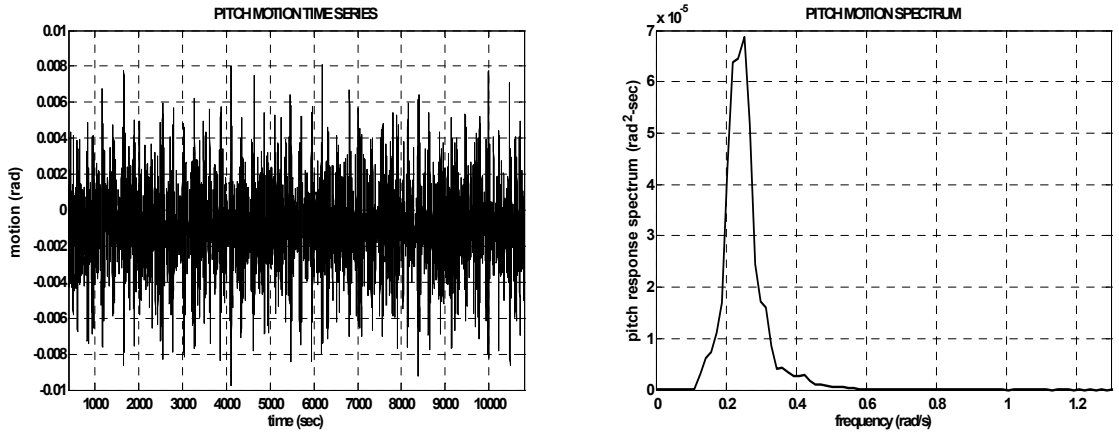

Fig. 28. Pitch response time series and spectrum (Hs = 1.7 m, Tp =25 sec, γ =6.0).

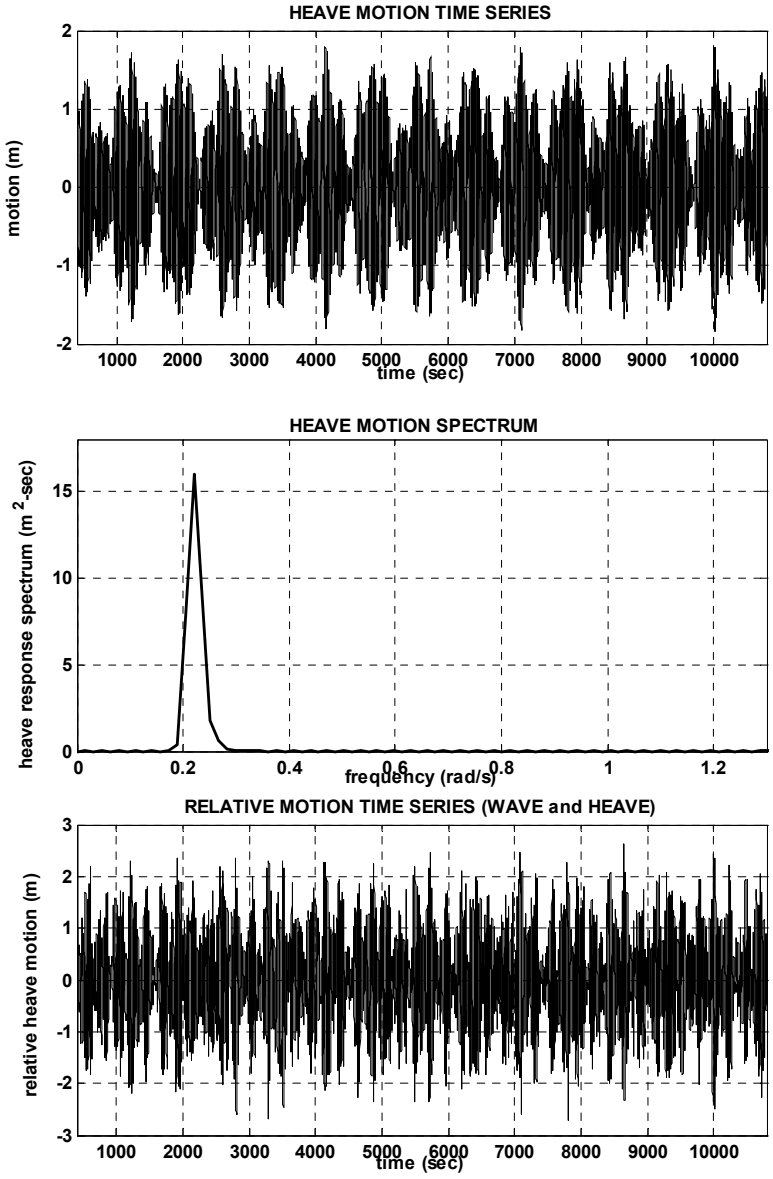

Fig. 29. Heave response time series and spectrum (Hs = 1.7 m, Tp =25 sec, γ =6.0).

Table 14. Summary of swell condition A statistics.

SWELL CONDITION A				
	SURGE (m)	**HEAVE (m)**	**RELATIVE HEAVE (m)**	**PITCH (deg)**
MEAN	-1.08E-03	-2.62E-03	-6.51E-03	-5.35E-02
STD	2.99E-01	6.31E-01	9.86E-01	1.98E-01
EXE	-1.06E+00	-1.68E+00	-3.36E+00	-6.80E-01
LF STD	6.65E-02	5.32E-02	-	4.03E-02
WF STD	2.87E-01	5.92E-01	-	1.90E-01
Notes:STD = standard deviation; EXE = extreme; LF = low frequency; WF = wave frequency				

Table 15. Summary of swell condition B statistics.

SWELL CONDITION B				
	SURGE (m)	**HEAVE (m)**	**RELATIVE HEAVE (m)**	**PITCH (deg)**
MEAN	1.00E-02	-3.37E-03	-5.10E-03	-5.32E-02
STD	2.31E-01	7.55E-01	9.36E-01	1.49E-01
EXE	7.86E-01	-1.84E+00	-2.71E+00	-5.61E-01
LF STD	5.60E-02	5.94E-02	-	4.55E-02
WF STD	2.17E-01	7.09E-01	-	1.38E-01
Notes:STD = standard deviation; EXE = extreme; LF = low frequency; WF = wave frequency				

Summary and Conclusions

Due to heave and pitch coupling of the spar platform in a nonlinear manner, the pitch restoring coefficient is a function of heave motion, and this can be expressed by the Mathieu instability equation. When the spar exhibits the Mathieu instability, the spar experiences lock-in phenomena in pitch motion. Depending on the amount of available damping, Mathieu instability may or may not occur. A damped Mathieu stability diagram is also developed in this study. The results of case studies can be summarized as follows:

First, a classical spar is modeled in a regular wave environment without considering the effects of the mooring lines and risers. The drag coefficient of the spar hull is changed to determine the effect of pitch damping on Mathieu instability. The simulation results clearly show the Mathieu instability mechanism as well as the pitch damping effects on the Mathieu instability. The Mathieu stability diagram also shows that increasing pitch damping suppresses the Mathieu instability problem.

Second, the same spar is modeled in regular waves, and the mooring lines and risers are considered. The results show that mooring line and riser buoyancy-can effects play an important role in the Mathieu instability analysis of a spar platform through increasing damping/shifting pitch natural period. Thus, the possibility of Mathieu instability is expected to be overestimated without proper modeling of riser buoyancy-cans and mooring lines in the computer simulations and in the model basin experiments.

Third, the wave elevation effect on the Mathieu instability is investigated. The simulation results show that wave elevation effect can be very important with large wave elevation and large phase difference between wave and heave motion. Thus, Mathieu instability analysis may be incorrect without considering wave elevation effect.

Fourth, the simulations are conducted for West Africa and North Sea swell environment conditions. The Swell-A and Swell-B simulation results show that for both cases the maximum heave motion is 1.7 ~ 1.9 meters (5.5 ~ 6.2 ft) and the maximum pitch motion is around 0.6 ~ 0.7 degrees. Based on the regular wave simulation results, the spar platform is very stable in this range of heave and pitch response. It shows that the spar platform does not experience Mathieu instability in the typical swell environment condition. However, the heave motion standard deviation in the swell condition is five times larger than that for the 100-year hurricane condition in the Gulf of Mexico. Due to small wave elevation in the swell environment, the wave elevation does not give significant effects on the Mathieu instability of the spar platform.

References

Cao, P., and Zhang, J., 1996. Slow motion responses of compliant offshore structures. Proceedings of the 6th International Offshore and Polar Engineering Conference, Los Angeles, vol. 1, pp. 296-303.

Haslum, H. A., and Faltinsen, O. M., 1999. Alternative shape of spar platforms for use in hostile areas. Proceeding of the 31st Offshore Technology Conference, Houston, pp. 217-228, OTC 10953.

Kim, M. H., 1997. WINTCOL/WINPOST User's Manual. Ocean Engineering Program, Civil Engineering Department, Texas A&M University, College Station, TX.

Koo, B. J., 2003. Evaluation of the effect of contact between risers and guide frames on offshore spar platform,Ph.D. Dissertation, Civil Engineering Department, Texas A&M University, College Station, TX.

Ma, W., Lee, M. Y., Zou, J., and Huang, E. W., 2000. Deepwater nonlinear coupled analysis tool. Offshore Technology Conference, (OTC 12085), Houston, TX.

Mekha, B.B., Johnson, C.P., and Rosset, J.M., 1995. Nonlinear response of a Spar in deep water: Different hydrodynamic and structural models. Proceedings of the 5th International Offshore and Polar Engineering Conference, Los Angeles, vol. 1, pp.462-469.

Prislin, I., Halkyard, J. E., DeBord, F., Collins, J. I., and Lewis, J. M. 1999. Full-scale measurements of the Oryx Neptune production spar platform performance. Proceeding of the 31st Offshore Technology Conference, Houston, pp. 209-215, OTC 10952.

Ran, Z., and Kim, M.H., 1997. Nonlinear coupled responses of a tethered Spar platform in waves. International Journal of Offshore and Polar Engineering, vol. 7, No. 2, pp. 111-118.

Ran, Z., Kim, M.H., Niedzwecki, J.M., and Johnson, R.P., 1995. Response of s Spar platform in random waves and currents (Experiment Vs. Theory). International Journal of Offshore and Polar Engineering, vol. 6, No. 1, p 27-34.

Rho, J. B., Choi, H. S., Lee, W. C., Shin, H. S., and Park, I. K., 2002. Heave and pitch motion of a spar platform with damping plate. Proceedings of the 12th International Offshore and Polar Engineering Conference, Kitakyshu,

vol. 1, pp. 198-201.

Rho, J. B., Choi, H. S., Lee, W. C., Shin, H. S., and Park, I. K., 2003. An experimental study for mooring effects on the stability of spar platform. Proceedings of the 13th International Offshore and Polar Engineering Conference, Honolulu, HI, vol. 1, pp. 285-288.

Tahar, A., Ran, Z., Kim, M.H., 2002, Hull/mooring/riser coupled spar motion analysis with buoyancy-can effect. Proceedings of the 12th International Offshore and Polar Engineering Conference, pp. 223-230.

Zhang, L., Zou, J., and Huang, E. W., 2002. Mathieu instability evaluation for DDCV/SPAR and TLP tendon design. Proceeding of the 11th Offshore Symposium, Society of Naval Architect and Marin Engineer (SNAME), Houston, pp. 41-49.